ADDIS ABEBA UNIVERSITY
COLLEGE OF NATURAL AND COMPUTATIONAL SCIENCE
SCHOOL OF EARTH SCIENCE

"APPLICATION OF GRAVITY, MAGNETIC AND ELECTRICAL RESISTIVITY METHODS FOR GEOTHERMAL INVESTIGATION AT THE CORBETTI CALDERA, MAIN ETHIOPIAN RIFT, ETHIOPIA"

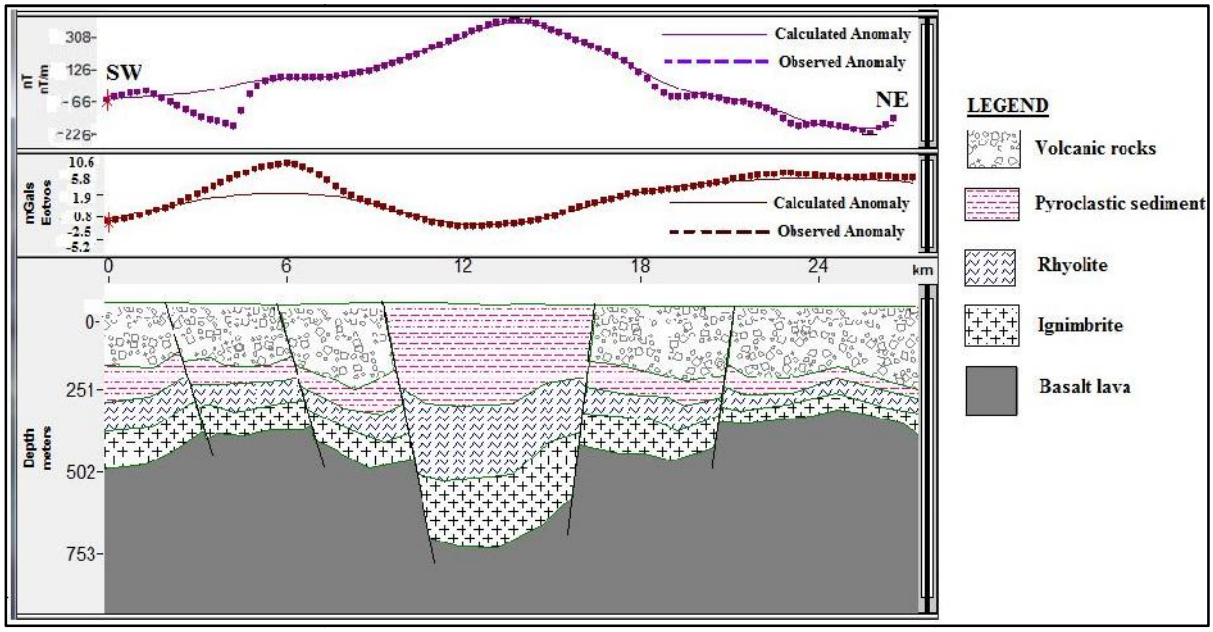

By: Bisrat Kebede

A Thesis submitted to the School of Graduate Studies, Addis Ababa University, in partial fulfillment of the requirements for the Degree Master of Science in Exploration Geophysics.

30 May 2006

ADDIS ABEBA UNIVERSITY

COLLEGE OF NATURAL AND COMPUTATIONAL SCIENCE

SCHOOL OF EARTH SCIENCE

"APPLICATION OF GRAVITY, MAGNETIC AND ELECTRICAL RESISTIVITY METHODS FOR GEOTHERMAL INVESTIGATION AT THE CORBETTI CALDERA, MAIN ETHIOPIAN RIFT, ETHIOPIA"

By: Bisrat Kebede

Approved by Board Examiners:

Dr. Seifu Kebede	----------
Chairman, School of Earth Science	Signature
Dr. Tarun Rajuvanish	----------
Chair person, Graduate Committee	Signature
Dr. Abera Alemu	----------
Advisor	Signature
Prof. Gezahegn Yirgu	----------
Co-advisor	Signature
Dr. Tigistu Haile	----------
Examiner	Signature
Dr. Dereje Ayalew	----------
Examiner	Signature

Declaration

I, the undersigned, declare that this thesis is my original work, has not been presented for degrees in any other University and all Sources of material used for the thesis have been duly acknowledged.

Name: Bisrat Kebede

Signature: _____

Date: _____

This thesis has been submitted for examination with my approval as a University advisor.

_____

Dr. Abera Alemu

_____

Prof. Gezahegn Yirgu

Acknowledgement

First and foremost I am grateful to my advisor Dr. Abera Alemu for his help during my field work, fatherly approach, encouragement, crucial comments and sound suggestions that he provided throughout my research work and also my Co-advisor Prof. Gezahagn Yirgu for his help in the research work.

Secondly, I would like to express my deepest gratitude to all staffs of Ethiopian Geological Survey for letting me to use all the necessary materials and data with all its staff members especially Ato Birhanu Bekele GSE, Department of Geothermics for his invaluable assistance concerning computer softwares. And also I would like to thanks Ato Yemanhe Kelemework graduate assistant, SES and Ato Elias Tadesse driver for their assistance during the field work activities.

Thirdly, persons who have had direct influence in doing this thesis through many days of Computer software training help discussion and reading were Eyasu leta, Fithat Habterweld and Belayaneh Dress. Thanks a lot friend!!!

Last but not least, my deepest heartfelt gratitude also goes to my family. Their care and encouragement has played an important role throughout my academic life.

Oh! One last thing, I have infinite gratitude to all of my instructors and colleagues in the School of Earth Sciences, AAU.

Table of Contents

List of Figures

Abstract

In this thesis work integrated geophysical techniques, involving electrical resistivity, gravity and magnetic surveys have been carried out over the Corbetti Caldera in the central Main Ethiopian Rift (CMER) to verify the geothermal potential of the caldera. Corbetti geothermal prospect is located about 250 km south of Addis Ababa and 20kms from Awassa and the area is bounded by Lake Awassa to the south and Lake Shalla to the north with geographic location between latitude 7.17^0N-7.25^0N and longitudes 38.30^0E-38.47^0E.

The Corbetti Caldera is characterized by Quaternary volcano tectonic activity which is mainly silicic volcanism and a resurgent caldera structural system. The Quaternary volcanism is associated with a wide spread of steaming ground and fumarolic activity which evidenced the existence of a heat source at depth.

56 VES points, 200 gravity and about 200 magnetic data have been used and analyzed and results are presented as magnetic, gravity and electrical counter map for qualitative interpretation and also gravity and magnetic 2-D model constrained with Geoelectric section for quantitative interpretation.

The complete Bouguer gravity anomaly in conjugation with total magnetic field anomaly map of the area indicates the existence of intrusion beneath the caldera, i.e. the highest Bouguer gravity anomaly resulting from the higher density of the intrusion correspondingly the shallower heat source caused by this intrusion is characterized by the lowest magnetic anomaly response.

Results from vertical electrical soundings along profile-2 indicates the presence of middle thicker conductive zone which is associated with the increase in temperature and alteration of rocks and apparent resistivity map for AB/2=1810m and AB/2=2700m shows low resistivity anomaly follows the eastern and northern caldera rim, stretching north of the caldera towards Lake Shalla.

Based on the joint analysis of data from these geophysical methods and thermal manifestations in the area, the area has the potential for large scale electrical power development. Besides, additional geophysical methods are proposed to further reinforce the outcome of the study.

CHAPTER ONE

1. INTRODUCTION

1.1 Background

The word geothermal comes from two Greek words geo, meaning earth, and therme, meaning heat. Geothermal energy is thus heat energy derived from the internal heat of the Earth. People around the world use geothermal energy to produce electricity, to heat homes and buildings, and to provide hot water for a variety of uses. Geothermal energy is therefore a clean renewable source of energy that is being used in many parts of the world having accessible geothermal resources.

A thinned and fractured crust allows magma to rise to the surface as lava flows. The greatest part of the magma does not reach the surface but heats large regions of underground rocks. Rainwater can seep down the faults and fractured rocks for miles. After being heated, it can return to the surface as steam or hot water. When hot water and steam reach the surface, they can form fumaroles, hot springs, mud pots and other interesting phenomena. Otherwise, when the rising hot water and steam is trapped in permeable and porous rocks under a layer of impermeable rock, it can form a geothermal reservoir. This geothermal reservoir could be a powerful source of geothermal energy. Geothermal reservoirs are associated with hydrothermal systems such as volcanoes and igneous intrusions related with hydrothermal zones (i.e., regions in the upper crust through which hot water has circulated). The origin of such reservoirs is hosted by volcanic rocks extruded into the upper crust at spreading centers (oceanic ridges and continental rift zones). At oceanic ridges (oceanic hydrothermal zones), the water may be seawater that penetrates into deep cracks. At continental rift zones, the water is provided by rainfall referred to as meteoric water. The water is commonly heated by magmatic intrusions, which cause it to expand and hence rise (Figure. 1.1).

A geothermal system is thus made up of four main elements: a heat source, a reservoir, a fluid, which is the carrier that transfers the heat, and a recharge area. The heat source is generally a shallow magmatic body, usually cooling and often still partially molten. The volume of rocks from which heat can be extracted is called the geothermal reservoir, which

contains hot fluids (vapor and gases). A geothermal reservoir is usually surrounded by colder rocks that are hydraulically connected with the reservoir. Hence water may move from colder rocks outside the reservoir (recharge) towards the reservoir, where hot fluids move under the influence of buoyancy forces towards a discharge area (Figure. 1.1).

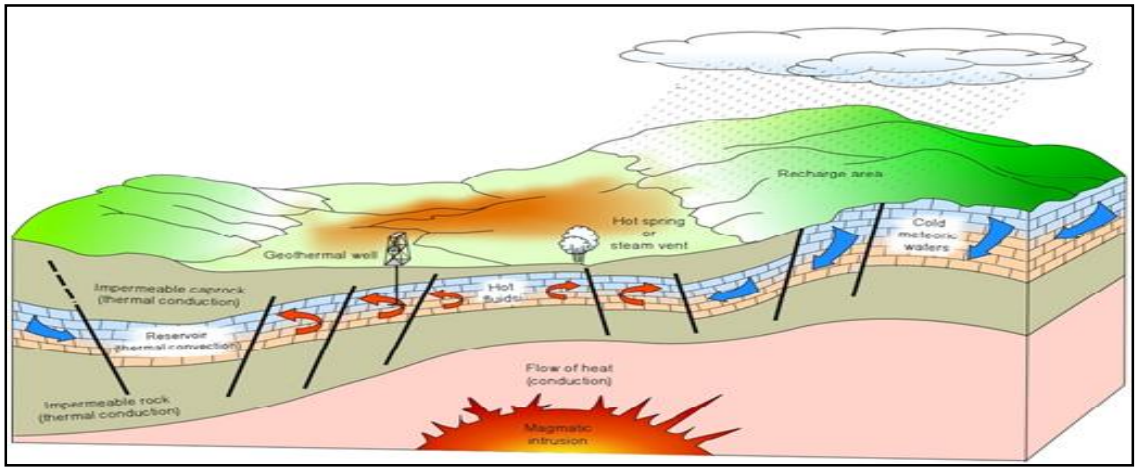

Figure 1.1 Schematic representation of an ideal geothermal system (Mary and Mario, 2004).

Geological, geophysical and geochemical surveys have remained to be the main survey types carried out for the assessment of the geothermal resource potential of the East Africa continental rift zones. Occurrences of geothermal resources associated with the central volcanoes in the Main Ethiopian Rift (MER) which forms one segment of the East Africa continental rift zones can be intensively studied using geological (structural mapping), integrated geophysical (gravimetric, magnetic, electrical, etc) and geochemical (water and gas analysis) method. The Corbetti volcano which forms one of the central volcanoes in the MER is the study area considered in this thesis research. Previous works performed to assess the geothermal resource potential of the Corbetti volcano included geological (structural mapping), geochemical (water and gas analysis) and geophysical (mainly gravity and electrical resistivity) investigations where magnetic data is lacking.

Based on geological (volcanolgical, stratigraphic, etc.) and geochemical evidences, the evolution of the Corbetti volcano is determined to be associated with extensive fractional crystallization of parent mantle-derived basaltic magma occurring in a huge shallow level

magma chamber. Fumaroles, steaming and warm grounds are some of the hydrothermal manifestations in the Corbetti Caldera (Elias Altaye, 1983). Drilling to locate fractured zones, or altered brecciate levels associated with sub-vertical faults of the Caldera has incurred high financial cost.

Integrated geophysical (gravity, magnetic and electrical resistivity) investigations (with the inclusion of new magnetic data independently acquired by this MSc project) are considered. The investigations are made to possibly identify and locate subsurface geological structures associated with hydrothermally altered volcanic lying within their unaltered equivalents residing at the Corbetti Caldera.

On geological, geophysical and geochemical grounds, the possible geologic structures and lithological features that may give rise to the anticipated gravity, magnetic and resistivity anomalies might include:

- A postulated intrusive body or magma chamber located at some depth below the Caldera fill,
- Hydrothermal alteration of the ferromagnetic minerals in the underlying rocks due to heat treatment
- Variations in rock physical properties of the Caldera fill that result mainly from:
- Mode of deposition and degree of compaction of sedimentary units associated the pre and post caldera sediments and recent alluvium.
- Emplacement of igneous rock units of contrasting physical properties
- Hydrothermal alteration of the local rocks by mineral deposition in pore spaces from hot hydrothermal solutions bearing dissolved minerals moving horizontally and vertically through porous zones (Locke and de Ronde, 1987).

This MSc research study aims at the application of gravity, magnetic and resistivity methods for detailed geothermal resource investigations of the Corbetti volcano. The study stems from the necessity to make effective use of geophysics based on modern data analysis and

interpretation knowledge for geothermal exploration. The outcome of the study may provide vital information to decide on the possibility of extending geophysical investigations for the assessment of the geothermal potential of the central volcanoes in the MER and for further scientific studies of rifting processes within the framework of global plate tectonics.

1.2 Location of the study area

The Corbetti geothermal prospect area is one of the geothermal prospect areas identified in the MER and the Afar depression (Fig. 1.2 A). It is located in the central part of the MER and approximately lies between latitudes 6.88^0N - 7.75^0N and longitudes 38.00^0E - 39.00^0E and about 250 km south of Addis Ababa along the Addis Ababa - Nairobi highway. The Corbetti geothermal prospect area encompasses an area of about 12100 km^2 within which Urji, Chebbi, Danshe and other volcanoes are consisted.

The Corbetti caldera that constitutes the present study area is bounded by Lake Awassa to the south and Lake Shalla to the north, with geographic locations between latitudes 7.17^0N - 7.25^0N and longitudes 38.30^0E - 38.47^0E (Figure 1.2 B).

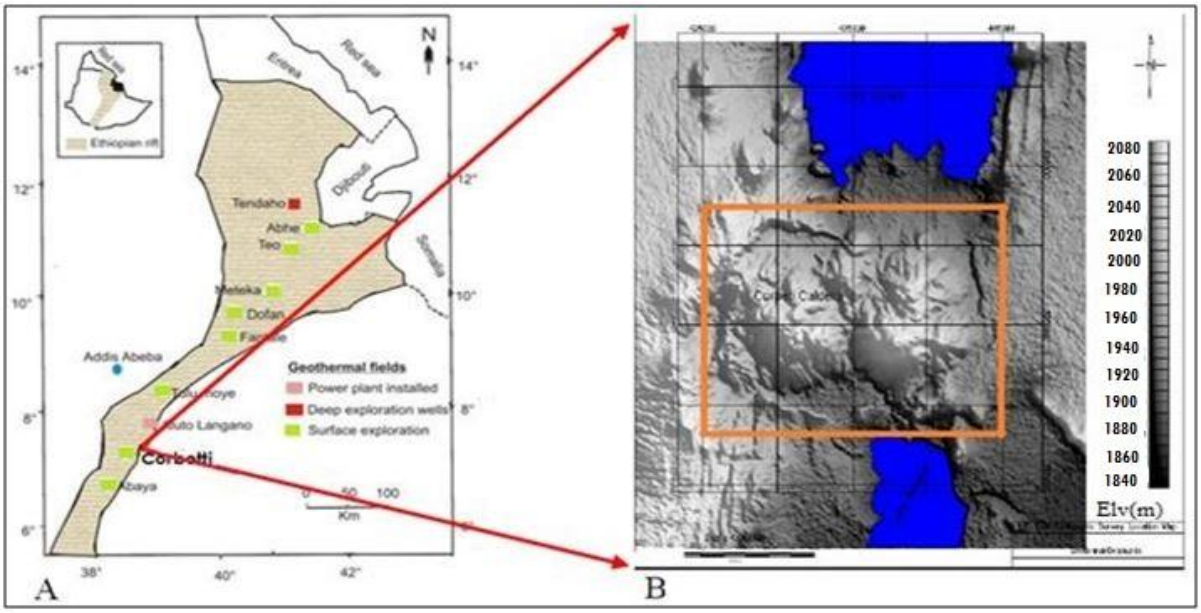

Figure 1.2 A: Location of the Corbetti geothermal prospect area within the geothermal prospect areas of the MER. B: Location of the Corbetti caldera within the Corbetti geothermal prospect area (MOM Report, 2008).

1.3 Relevance of the proposed study

Geothermal deposits provide an important contribution to the world's energy production, this class of deposits has recently become a focus attention for the exploration of geothermal resources at magmatic centers of continental rift zones (MOM Report, 2008). This MSc research aims at the application of gravity, magnetic and electrical resistivity methods for detailed geothermal resource investigations of the Corbetti Caldera. The study stems from the necessity to collect new magnetic data that fills the missing magnetic data coverage over the volcano in order to make an effective use of geophysics for geothermal resource potential assessment tasks based on modern geophysical data analysis and interpretation techniques. The outcome of the study may provide vital information to decide on the possibility of extending the geophysical investigations considered here for the assessment of the geothermal potential of the central volcanoes in the MER and the Afar depression.

1.4 Objectives

1.4.1 General Objective

The general objective of this MSc thesis is to properly utilize and analyze the present geophysical studies and integrate them with the previous geophysical and geological study results in order to delineate and map the prominent geological features, structural features and volcanologic features of the Corbetti caldera that are thought to be the controlling factors in the assessment of geothermal resources.

1.4.2 Specific objective

- Systematic mapping and analysis of thermally altered zones of Corbetti caldera to serve as a guide to delineating areas of varying hydrothermal activities.
- Defining the vertical geoelectric section of the study area.
- Preparation of 2-D gravity and magnetic models constrained by geoelectrical (VES) data for the study area.

- To acquaint oneself with the methods of geophysical data acquisition, interpretation and presentation of results.

1.5 Methodology

Geophysical methods are applied in a wide variety of problems; they are used for oil and mineral prospecting, for solving groundwater, geothermal and engineering problems. Moreover, geophysics plays a fundamental role in studies of the Earth's deep interior otherwise inaccessible by other means.

Although the location of a geothermal field is controlled by the regional geology, its characteristics, as recognized at the surface through the geothermal exploration techniques, are essentially hydro geological phenomena. They depend not only on suitable heat source but also on the presence of a medium (normally water) in which the heat can be transported to the surface and on a permeable path along which the medium (the fluid) can travel. In simple terms, the recipes for a geothermal system are: large source of heat, a reservoir to accumulate heat, a barrier to hold the accumulated heat and adequate supplies of water such as ancient connate, magmatic waters or more recent juvenile and meteoric waters (MOM Report, 2008).

This research plans to integrate existing surface geological and hydrogeological maps and other relevant information with subsurface geophysical investigations in order to study the component parts directly or indirectly.

The gravity method would be used to map regional geological structures and intrusion in the area and the magnetic method would map the major structures that are paths for the rising heat to shallow depths to interact with the down flowing waters in the aquifer zone. The deep electrical sounding surveys would establish the vertical stratification of the geoelectric layers of the area.

- The flowchart of the general methodologies that will be implementing is shown below.

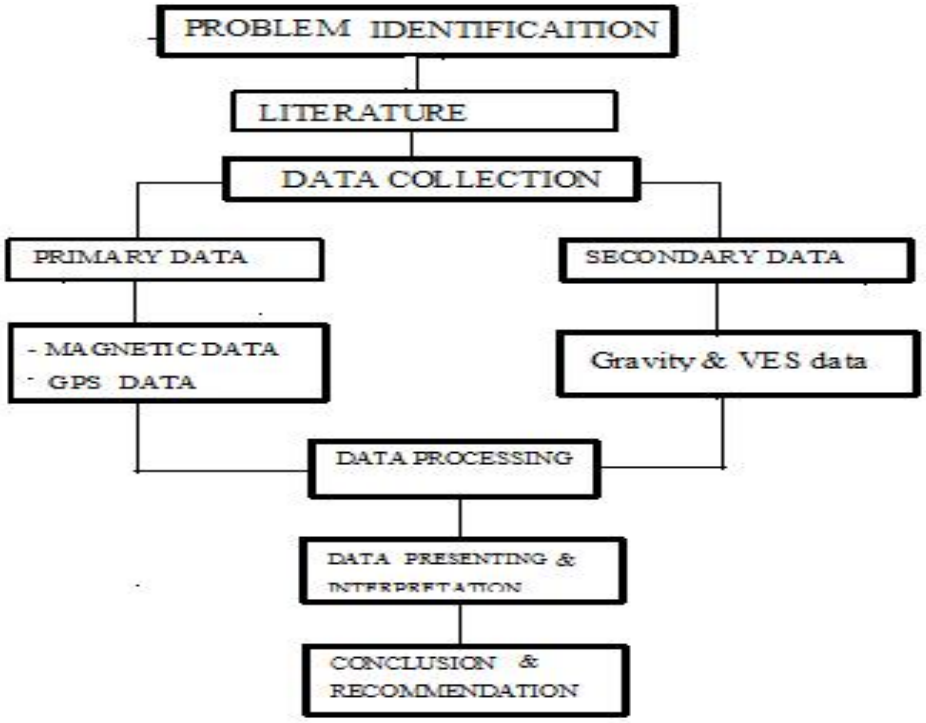

Figure 1.3 The general methodology and the data organization flow chart

1.6. Review of Previous Work

The Corbetti has been studied for different purpose since (Mohr, 1966) and Macdonald and Gibson (1969). But the initial stage of the geothermal exploration started by the joint studies of the EIGS and the UNDP technical teams (UNDP, 1973). Then followed by Lloyd, 1977, which indicated the presence of a geothermal resource and recommended future detailed geoscientific study which includes among others, detailed geological and surface hydrothermal alteration study on 1:50,000 and 1:20,000 scales. Detailed geological and surface hydrothermal alteration study on 1:50,000 scales were conducted by Elias Altaye (1983-1984). Temperature measurements and associated hydrothermal alteration studies in Corbetti geothermal prospect are carried out by MoME and GSE, 2011. The present study is a continuation of the above studies.

1.7. Structure of the Thesis

This thesis is organized in to five chapters. The first chapter is general introduction of the study. The second chapter discusses previous geological works of the MER as well as the study area. The third chapter addresses the theoretical backgrounds of the geophysical methods employed in this study. In the fourth chapter, compilation of the different maps and models and their qualitative and quantitative descriptions are presented. The fifth chapter presents conclusions and recommendations of the work. Lastly reference materials used for this work are listed alphabetically.

CHAPTER TWO

2. GEOLOGICAL AND TECTONIC REVIEW

2.1. Geological and Tectonic setting of the Main Ethiopian Rift

The term Ethiopian Rift system is used to designate the three discrete Rift segments, namely the Afar depression, the Main Ethiopian Rift (MER) and the Southern Ethiopian Rift (SER). This rift system is part of the great East African Rift System (EARS), widely believed to have been formed by diverging lithospheric plates, active since early Tertiary times. The Great East African Rift itself is part of the Afro-Arabian Rift system that extends for about 6500km from Turkey to Mozambique (Mohr, 1962).

Flood basalts erupted primarily between 31–29 Ma cover much of the Proterozoic basement, extending over an area of the Ethiopian plateau ~1000 km in diameter (Baker et al., 1996; Hofmann et al., 1997; Ukstins et al., 2002). A mantle slow-velocity anomaly underlies the rift (Bastow et al., 2005; Benoit et al., 2006; Montelli et al., 2006) down to at least 650 km depth beneath Afar and rising to at least 75 km depth beneath the Main Ethiopian Rift. The shallow part of this anomaly is offset ~25 km from the rift axis (Bastow et al., 2005) and dips westward, possibly connecting to the African Super plume (Benoit et al., 2006) although direct evidence remains elusive.

The MER has traditionally been divided into three sectors based on surface geology and geomorphology, the northern (NMER), central (CMER), and southern (SMER) sectors. The NMER extends south from the Afar depression to near Lake Koka, with border faults that trend on average at N50°E and have formed since 10–11 Ma. Early volcanism also began at 10–11 Ma (Chernet et al., 1998; Wolfenden et al., 2004). The CMER extends from Lake Koka through the lakes region to Lake Awasa, with border faults trending on average N30°E–N35°E. The age of onset of extension in the CMER is still debated. Wolde Gabriel et al. (1990) estimate the age of onset of faulting to be 8.3–9.7 Ma with earliest synrift volcanics at ~8 Ma, whereas Bonini et al. (2005) estimate the onset of extension and initial volcanism to be 5–6 Ma. The SMER extends south from Lake Hawasa into the broadly rifted zone of southern Ethiopia (Ebinger et al., 2000) with faults trending north–south to N20°E.

Faulting in the SMER was well established by ~18 Ma (Ebinger et al., 1993; Wolde Gabriel et al., 1991), and volcanism began around 18– 21 Ma (Ebinger et al., 1993; George and Rogers, 2002).

The Main Ethiopian Rift (MER), being one segment of the East African continental rift system is characterized by recent volcano-tectonic features (central volcanoes, calderas, craters, cones, faults, grabens, etc), intense seismic activity and zones of mineralization with possible shallow intrusions. Several Quaternary central volcanoes namely Corbetti, Aluto, Gedemsa, Dofan, etc. (Fig-2.1) are present along the axial portion of the MER (a continental spreading center). These central volcanoes offered opportunities for potential geothermal resource investigations. The Corbetti volcano, a central volcanic complex in the MER, is among those promoted for detailed geothermal resources investigation.

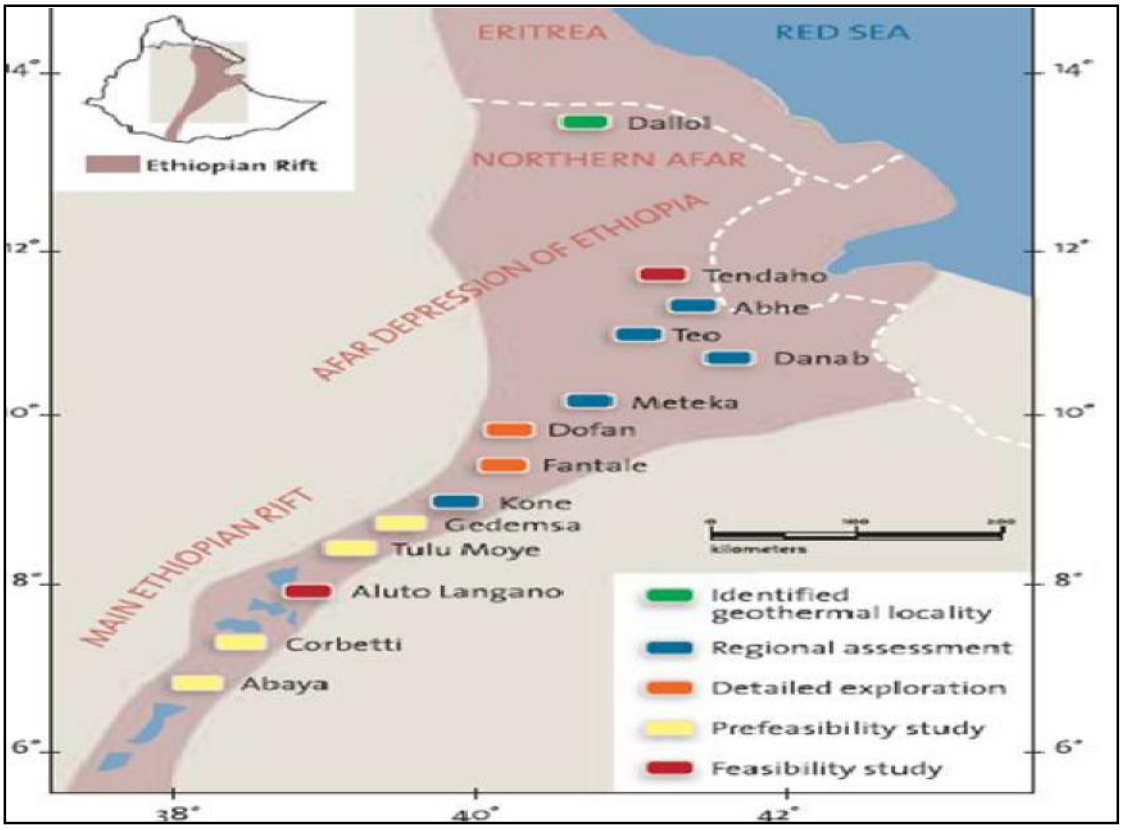

Figure 2.1 Location map of the geothermal prospect areas within the Ethiopian Rift Valley (after Meseret Teklemariam, 2000)

2.2. Geological Setting of the study area

The Main Ethiopian Rift is divided based on structural features into three geographic areas; represented by the northern (Fentale Nazret), Central (Nazret Hawassa) and Southern (Hawassa-Konso) sectors. The central sector, where the Hawassa lake basin belongs to is a symmetric rift basin where both sides of the rift margins are fully defined except in the region between Guraghe and Sodo of the western escarpment and the Shashemene area of the eastern margin, (Taddesse and Zenaw 2003). The closed basin of the nested Hawassa-Corbetti caldera complex is a giant elliptical depression 30-40kms wide.

Post caldera activity around Corbetti area is represented with the birth of three recent peralkaline volcanoes (Urji, Chebbi and Danshe). The Corbetti caldera is elliptical in shape; the minor axis is about 10km N-S and the major axis is about 18km E-W.

As to the geological compositions, it is within recent volcano tectonic activities on Wonji Fault Belt, mainly composed of per alkali-silicic products, rhyolite flows, obsidians, pumice, ashes, ignimbrites and the same nature of basaltic lava flows and scoria. There are pre and post caldera sediments and recent alluvium. All volcanic formation indicates starting from early formation of the caldera to the plio-pleistocene activities which are characteristics of the MER (Elias Altaye, 1983).

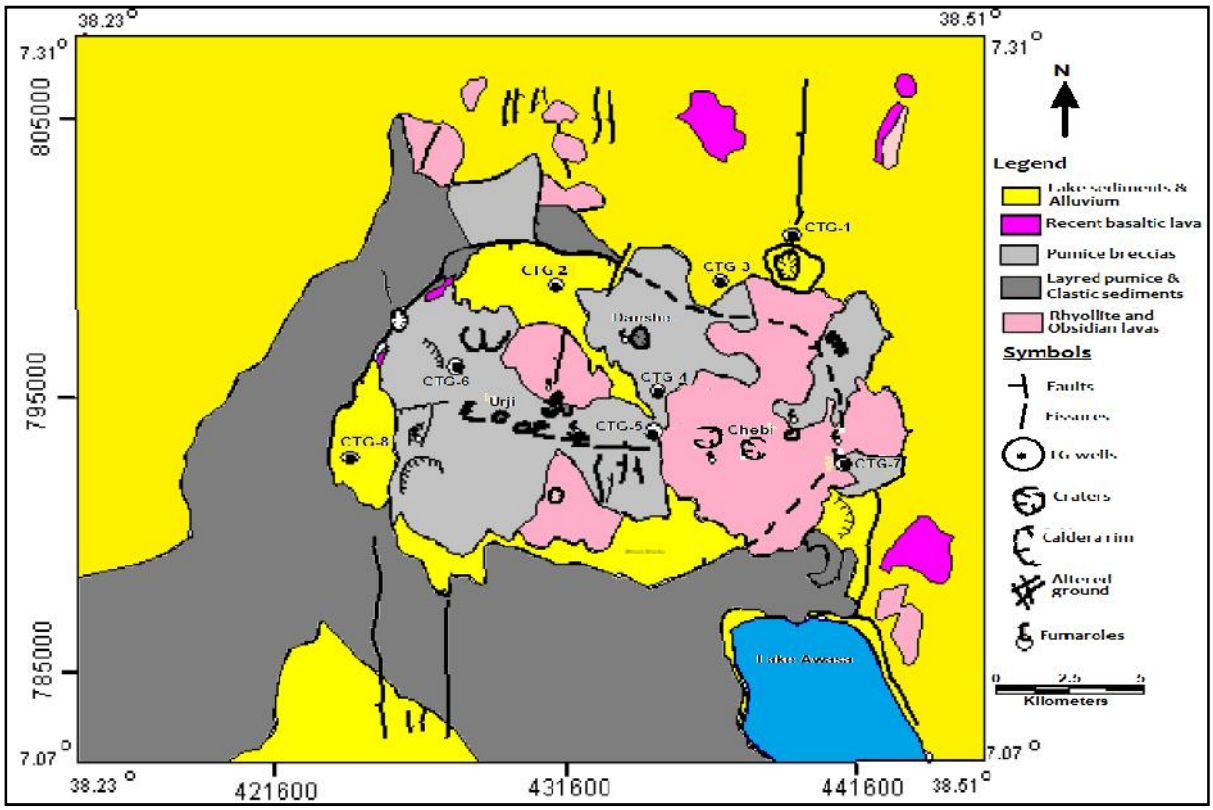

Figure 2.2 Simplified geological map of Corbetti area **(**modified from Tadesse Mamo and Zewdu Abtew, 2011)

The caldera comprises fissure eruptions, which were followed by a volcano-tectonic collapse. The volcanoes are all at a fumarolic stage. Urji and Danshe volcanoes are formed of pyroclastics which are represented by pumice falls; on the eastern side of Urji some obsidian enter bedded with pumice outcrop. Chebbi volcano is mostly formed of pumice like Urji. The difference between the three volcanoes is the amount of very recent obsidian lava flows which cover the pyroclastics of Chebbi (Di Paola, 1972).

Chabbi volcano is extruded from the eastern segment of the caldera ring fractures, but east west tectonics may also be an important factor controlling its location. The east west alignment evident on Urji is even more evident on Chebbi because the pyroclastic over burden is less or absent. Present east-west sub-parallel fissure swarms cut the lava flows independent of their flow direction and are probably the surface expression of deep tectonic

weakness evidenced also by a major east-west fault, down thrown south, which appears east of Chebbi and gains topographic expression east wards (UNDP Technical Report, 1973).

There are many occurrences of fumaroles (steam vents) and hot ground (hot springs) in several places within the caldera. In general most of the hydrothermal manifestations are associated with recent volcanological fractures such as eruption centers, craters and caldera rims, controlled by structural features (faults, fissures, joints and contact zone). Hydrothermal manifestations i.e., altered ground with fumarolic activities are associated with fissures, craters, faults and caldera rims, where tectonic structures give major access for hydrothermal fluids.

These zones of fumeroles and structural features are supposed to be favorable zones for potential mineral deposit like epithermal Gold, Sulfides, etc. and also geothermal resource area which usually are zone of alterations.

Corbetti is a silicic volcanic system similarly to Alutu volcano, except for it's being a well developed resurgent cauldron system. Corbetti caldera has an irregular elliptical outline, elongated in the east-west direction and measuring 10 and 15 km along its two axes. The eastern rim of the caldera is missing, most likely due to the eastern part of the parent volcano having been completely removed during caldera formation. The -caldera-forming volcano developed on terrain made up of late Tertiary ignimbrites. Later ignimbrites, which led to the collapse of the caldera, form the present rift floor surface in the area and the flanks of the caldera that are still intact. On the volcanic edifices situated inside the caldera, fissures oriented in the E-W direction cross, NNE-SSW trending regional rift forming faults. The results of geological study could be summarized as follows:

The volcanic products at Corbetti are very young. The repeated cycle of volcanism forming the present morphology of Corbetti system normally shall have remnant magma intruded at shallow depth. This young and shallow magmatic chamber at shallow depth is providing the heat to the Geothermal System at Corbetti.

The study of hydrothermal alteration minerals on the cuttings recovered from the shallow wells showed the presence of high temperature mineral assemblages such as chlorite, kaolin, calcite and quartz (Kebede et al, 1987 as cited in MoME, 2008).

Corbetti has a similar geological set up with that of Aluto-Langano. The caldera-forming volcano developed on terrain made up of late Tertiary ignimbrites which are the main reservoir rocks at Aluto-Langano. The annular structural configuration of the caldera is complicated by the existence of a dense set of the rift forming faults in the NNE-SSW direction. Transversal E-W oriented fissures and the NNE-SSW rift forming faults control the occurrence of hydrothermal features. This relatively pronounced structural fabric system compared to Aluto-Langano is expected to form relatively high secondary permeability in the Tertiary ignimbrites.

An extensive cap rock having large lateral coverage exists at Corbetti in the form of lake sediments and associated overlying pyroclastics. These cap rocks serve to prevent the heat of the Corbetti system from escaping to the surface, thus insuring a minimal cooling rate to the heating system.

Corbetti is considered to be a classic resurgent cauldron system post-caldera volcanism during the Pleistocene having produced four major volcanic edifices Urji, Chebi, Danshe and Borena. Urji occupies the center of the caldera. Chebi and Borena occupy an inferred eastern caldera rim, being products of post caldera resurgence of volcanism along possible ring fractures. Danshe and other low lying eruptive centers such as Hare and Guge probably stand on ring fractures skirting the interior of the caldera in the Northeast and west.

CHAPTER THREE

3. THEORETICAL BACKGROUNDS IN GEOPHYSICAL METHODS

3.1 Introduction

In exploration Geophysics, there are different geophysical methods that respond to the physical properties of the sub-surface media. These geophysical methods can be classified into two broad groups. The passive methods, those that detect variation within the natural fields associated with the earth; such as gravitational and magnetic fields. And the active methods, those that use artificially generated sources such as electrical methods, seismic methods and others. To locate and map a geothermal system, the system must then have anomalous physical properties different from those of the surrounding country rocks.

Geophysical methods play a key role in geothermal exploration since many objectives of geothermal exploration can be achieved by these methods. The geophysical surveys are directed at obtaining indirectly, from the surface or from shallow depth, the physical parameters of the geothermal systems. As it is clearly stated on the preceding chapter, chapter one this research plans to carry out an integrated geophysical survey through using magnetic, gravity and electrical methods.

In general, the gravity method is used in mapping regional geological structures at large scale. The magnetic and the gravity methods are known to complement each other and therefore the magnetic method is also used in mapping the major lithologic and structural units residing in the study area. The electrical resistivity methods would help to conduct a detailed structural analysis of the prospect area that helps locating the more permeable zones of geothermal reservoir and establish the vertical stratification of the geoelectric layers in the study.

3.2 The Gravity Method

3.2.1 Introduction

Gravity surveying measures variations in the Earth's gravitational field caused by differences in the density of sub-surface rocks. Although known colloquially as the 'gravity' method, it

is in fact the variation of the acceleration due to gravity that is measured. The gravity method is a potential field method that is based on the earth's gravitational field. Gravity methods have been used most extensively in the search for oil and gas, particularly in the twentieth century. While such methods are still employed widely in hydrocarbon exploration, many other applications have been found, some examples of which are, Regional geological studies, Isostatic compensation determination, Exploration for, and mass estimation of, mineral deposits, Monitoring volcanoes ..Etc (Reynolds, 1997). The method of gravity survey in geophysics involves measurement, reduction, mapping, and interpretation of gravity data (Dobrin, 1988). Gravimetry is the method of measuring and modeling the gravity field of the Earth (Torge, 1989).

3.2.2 Fundamental Principles of Gravity

The basis of the gravity survey method is Newton's Law of universal Gravitation and Newton's second law of motion. The law of universal Gravitation which states that the force of attraction $\vec{F}$ between two masses m_1 and m_2 , whose dimensions are small with respect to the distance *r* between them, is given by;

$$\vec{F} = \frac{-Gm_1m_2}{r^2}\hat{e} \qquad 3.1$$

where, F- is the force of attraction between m_2 and m_1

G - Is the gravitational constant which is equal to $6.67x10^{-11}m^3/kg.s^2$.

$\hat{e}$- Is a unit vector whose direction is the line connecting the centre of the two masses.

r - Is the distance between the two masses m_1 and m_2.

According to Newton's 2nd law of motion, the force (F), the mass (m) and the acceleration (a) or the gravitational acceleration (g) are related by

$$\vec{F} = \frac{-Gm_1m_2}{r^2}\hat{e} = m_2a \qquad 3.2$$

For the case of the earth of mass M_e and a body of mass, m located on or in the vicinity of its surface:

$$\vec{F} = \frac{-GM_e m}{r^2}\hat{e} = mg \qquad 3.3$$

From equation (3.3) above;

$$\vec{g} = \frac{-GM_e}{r^2}\hat{e} \qquad 3.4$$

g – Is gravity or gravity acceleration. The unit of 'g' is Gal in the honor of Galileo Galili. 1 Gal = 1 cm /s2. In geophysics we also use auxiliary units like milliGal. (mGal), micro Gal and so on. But the mGal unit commonly used; 1mGal =10-3cm/s^2.

3.2.3 Theoretical Gravity of the Earth

Considering a small mass, m moving with a velocity, **v** on the surface of the earth rotating with angular velocity, **ω** as shown in the Figure 3.1.

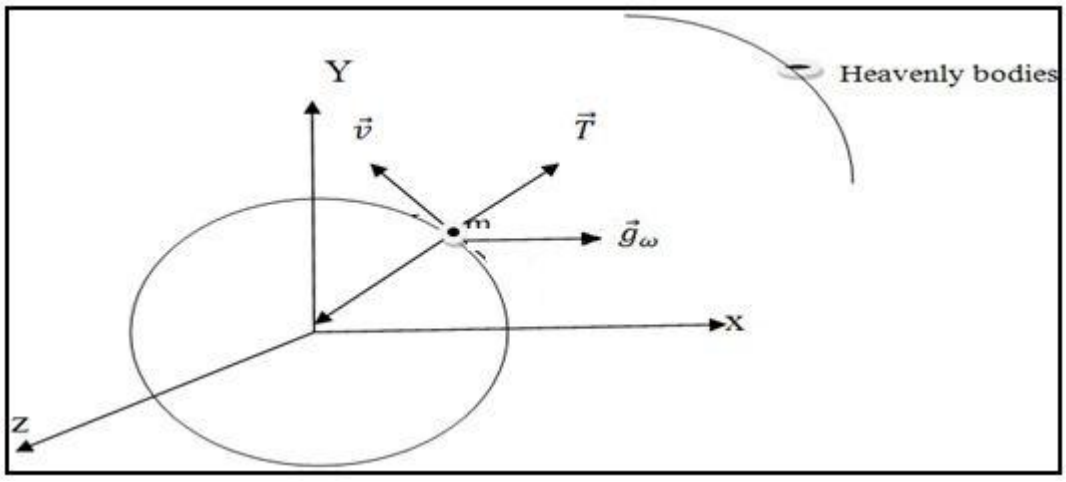

Figure 3.1 Modeling gravity (gravity force per unit mass acting on a mass, m on earth

From the figure 3.1 the resultant force per unit mass (acceleration) acting on a mass **m** is given by;

$$\vec{g} = \vec{g}_m + \vec{g}_\omega + \vec{g}_c + \vec{f} \qquad 3.5$$

where $\vec{g}_m$ - Attraction force per unit mass acting on m due to earth's mass.

$\vec{g}_\omega$ - Centrifugal force per unit mass acting on m due to earth's rotation with **ω**.

$\vec{g}_c$- is the Coriolis force per unit mass acting on m due to its linear velocity **v** on the surface of the Earth.

$\vec{h}$- is Tidal force per unit mass acting on m due to attraction of other heavenly bodies.

Assuming the Earth to be spherical in shape with radius (R), then from equation (3.4), the mass gravitation is given by;

$$\vec{g}_m = \frac{GM}{R^2} \qquad 3.6$$

The centrifugal acceleration $(\vec{g}_\omega)$ is given by;

$$\vec{g}_\omega = \vec{\omega}(\vec{\omega} \times \vec{R}) \qquad 3.7$$

Since it is not easy to express $\vec{h}$ with a simple formula and by considering the mass (m) is at rest on the surface of the Earth (V=0), the effects of $\vec{h}$ and $\vec{g}_c$ is considered negligible. Therefore the gravity $\vec{g}$ refers to the combined effect of both Earth's mass gravitational acceleration and rotational (centrifugal) acceleration, that is;

$$\vec{g} = \vec{g}_m + \vec{g}_\omega \qquad 3.8$$

That is;

$$\vec{g} = \frac{GM}{R^2}\vec{e}_r + \vec{\omega}(\vec{\omega} \times \vec{R}) \qquad 3.9$$

3.2.4 The Major Forces Acting on a Body on the Earth's Surface

The major force on a unit of mass at a point **p** on the surface of the earth is the centrifugal acceleration $\vec{g}_\omega$ and the mass gravitation acceleration $\vec{g}_m$ as shown in the figure below

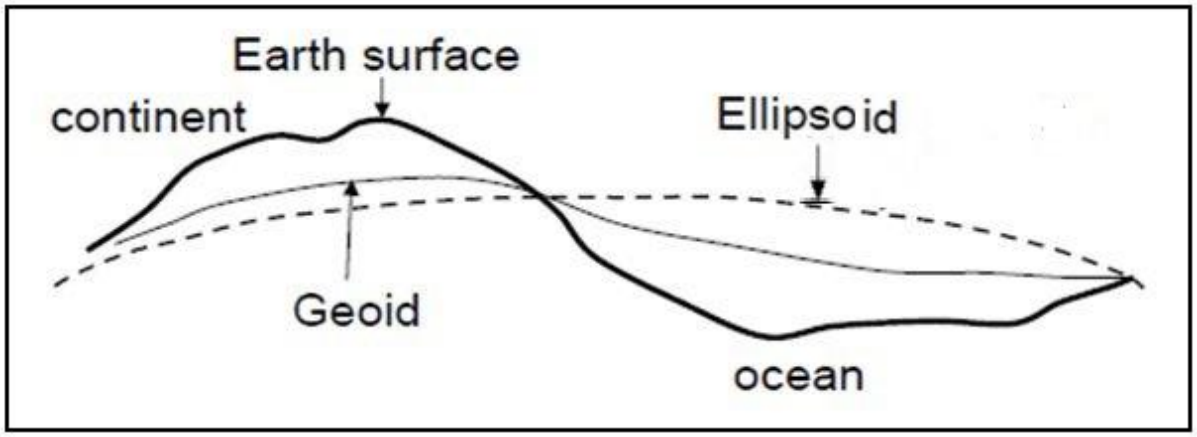

Figure 3.2 The major force acting on a per unit mass **m** on the surface of the earth.

From the figure above the resultant gravity force per unit mass is given by

$$\vec{g} = \vec{g}_m + \vec{g}_\omega \qquad 3.10$$

Since the centrifugal force per unit mass $\vec{g}_\omega$ is perpendicular to the rotational axis (ω) is given by the equation

$$\vec{g}_\omega = \vec{\omega}(\vec{\omega} \times \vec{R}) \qquad 3.11(a)$$

$$\vec{g}_\omega = \omega^2 R cos\phi \qquad 3.11(b)$$

The radial component of the centrifugal force per unit mass $\vec{g}_{\omega r}$ which is pointing along r is given by the equation

$$\vec{g}_{\omega r} = \vec{g}_\omega cos\phi \qquad 3.12$$

$\vec{g}_{\omega t}$ Which the tangential component is of has no effect on mass, m.

Substituting equation 3.11(b) into equation 3.12 the radial component of $\vec{g}_\omega$ pointing along r is given by as follow

$$\vec{g}_{\omega r} = \vec{g}_{\omega} cos\phi \qquad 3.13(a)$$

$$\vec{g}_{\omega r} = (\vec{\omega}^2 R cos\phi) cos\phi \qquad 3.14(b)$$

$$\vec{g}_{\omega r} = \vec{\omega}^2 R cos^2\phi \qquad 3.14(c)$$

Since the centrifugal force per unit mass $\vec{g}_{\omega}$ is radially outward from the surface of the surface of the earth and the mass gravitational force per unit mass $\vec{g}_m$ is toward the center of the earth, the resultant gravitational force acting on a unit mass on the surface of the earth is given by

$$\vec{g} = \vec{g}_m - \vec{g}_{\omega r} \qquad 3.15$$

Therefore;

$$\vec{g} = \frac{GM}{R^2} - \vec{\omega}^2 R cos^2\phi \qquad 3.16$$

- At the equator ($\phi = 0^0$)

$$\vec{g} = \vec{g}_e = \frac{GM}{R^2} - \vec{\omega}^2 cos^2$$

$$\vec{g}_e = \frac{GM}{R^2} - \vec{\omega}^2 R \qquad 3.17$$

- At the pole ($\phi = 90^0$)

$$\vec{g} = \vec{g}_p = \frac{GM}{R^2} - \vec{\omega}^2 cos^2 90^0$$

$$\vec{g}_p = \frac{GM}{R^2} \qquad 3.18$$

From equations (3.12) and (3.13) one can conclude that gravity value, g is minimum at the equator and maximum at the poles; but for the real Earth observed values of gravity, $\vec{g}$ at the poles and equator are g_p= 983.218 Gals and g_e = 978.032 Gals respectively. The difference between g_p and g_e yields about 5.2 Gals ($g_p - g_e$= 5.2 Gals) and calculations on a theoretical basis for a spherical Earth model is about 3.4 gals ($g_p - g_e = \omega^2 R$=3.4 Gals). The disagreement between observed values of gravity g for a real Earth and the calculated value of gravity, g for a spherical model Earth is due to the assumptions used above. From these disagreements one can conclude that;

- The shape of the real Earth is not spherical.
- The shape of the Earth is rotationally distorted one such that its shape is flattened at the poles and bulged at the equator.
- Gravity value, g varies as a function of latitude, ϕ

3.2.5 The Geoids and the Reference Ellipsoid

The Earth's shape is nearly spherical with a radius of about 3,963 miles (6,378km), and its surface is nearly irregular. Mountains and valleys make actually measuring this surface impossible because an infinite amount of data is needed. To measure the Earth's gravity field, shape and size and to avoid these problems, Geodesist and Geophysicists consider two surfaces that represent the average shape of rotationally distorted real earth to study its gravity field, shape and size. These are the geoids and the reference ellipsoid.

i. **The Reference Ellipsoid.**

An idealized geometrical or mathematically generated theoretical Earth model flattened at the poles and bulged at the equator. This model of the earth assumes no undulations on the Earth's surface where as we have hills, mountains and depressions on the real Earth. It also considers only radial variations in density of the Earth plus centrifugal acceleration. A theoretical Earth model up on which the variation of gravity, g with latitude (ϕ) is computed according to an international agreements in 1967 by IUGG as:

$$\gamma = g_e(1 + c_1 sin^2\phi + c_2 sin2\phi) \qquad 3.19$$

Where g_e = 978.0490, and

C_1 = 0.0052884
C_2 = 0.0000059

ii. **The Geoid.**

The geoid is the surface of constant potential energy that coincides with mean sea level over the oceans. A physical surface on earth referred to the mean sea level that must be related to the reference ellipsoid for its practical work. The geoid is a practical surface on which g values observed on the actual to topography of the real earth are mathematically shifted to its surface using gravity reduction methods which we are going to discuss later. Unlike the references ellipsoid, the geoid shows wide undulations following topography of real Earth. And also the geode considers both radial and lateral variation in density of the Earth and centrifugal acceleration.

3.2.6 Gravitational potential

By virtue of its position in the gravitational field of the Earth, the gravitational potential energy U of a test mass m at a distance r from the surface of the Earths' mass M that is assumed to be concentrated at its center is;

$$u = \frac{GMm}{r} \qquad 3.20$$

If the test mass m moves to a new position r' toward M, the work done in bringing the test mass to this new position is given by

$$W = \Delta U = \frac{GMm}{r'} - \frac{GMm}{r} \quad 3.21$$

Because the gravitational field is conservative, the work done moving a mass in a gravitational field is independent of the path traversed and depends only on the end points.

The gravitational force is a vector whose direction is along the line joining the centers of the two masses. The force giving rise to a conservative field may be derived from a scalar potential.

$$\Delta u(r) = g(r) \quad 3.22$$

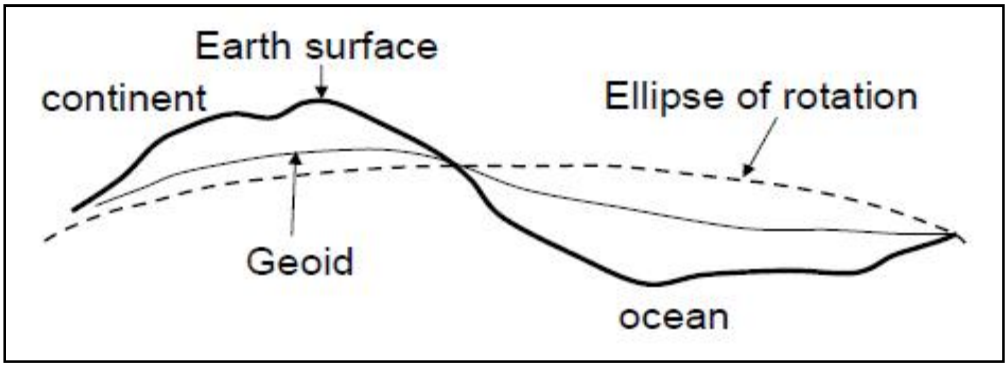

Figure 3.3 diagram representing potential surfaces of Geoid and Ellipsoid

For practical work measurements of Gravity is carried on the physical equipotential surface i.e. Geoid. The Gravity potential on the reference Geoid (Figure 3.3) given by;

$$W = W(x, y, z) \quad 3.23$$

For theoretical work gravity is calculated on the theoretical equipotential surface, i.e. Ellipsoid. The gravity potential on the reference Ellipsoid (Figure 3.3) is given by;

$$U = U(x, y, z) \quad 3.24$$

Since that the Ellipsoid and Geoid coincide at mean sea level we consider that they have the same potential U_O , that is;

$$W = W(x, y, z) = U(x, y, z) = U_O \quad 3.25$$

The value of gravity observed (g_o) on the Geoid surface thus determined by;

$$g_o = \frac{\partial U_O}{\partial z} \quad 3.26$$

The value of gravity calculated (γ) on the Ellipsoid surface is also determined by;

$$\gamma = \frac{\partial U_O}{\partial z} \tag{3.27}$$

And finally the formula to find theoretical gravity value, g at any point on the ellipsoid was adopted by International Union of Geophysics and Geodesy in 1967, as:

$$\gamma_{1967=} 978031.85(1 + 0.0053024sin^2\phi - 0.0000059sin^2 2\phi)mgal \tag{3.28}$$

Therefore gravity anomalies Δg is defined as the difference between g_o and γ as given by;

$$\Delta g = g_{o-}\gamma \tag{3.29}$$

where, g_o is observed gravity value of a certain station.

Gravity anomalies Δg also known as point gravity anomalies are developed as a consequences of difference in density distribution of the Earth particularly in the upper layer known as the crust. Therefore, they reflect the internal constitution of the Earth's crust and structural features such as faults, lineament, fissures etc of the Earth and resource potential hazard including hazard mitigation assessment tasks.

3.2.7 Gravity Reductions

The value of gravity on the mean sea level reference Ellipsoid vary with latitude (ϕ) to account for Earth's flatting and rotation according to the theoretical gravity formula equation (3.28), considering that the interior of the Earth is uniform but in practice, it is not possible to measure on the mean sea level reference Ellipsoid at the place where the theoretical gravity value γ is known. Gravity survey is takes place on the actual surface of the Earth where various topographical environments such as mountains, flatlands, ocean basins, etc causes the gravity g values differ from place to place. The readings will generally be influenced by latitude, tidal effect and instrumental drift, elevation and topography. To reduce them to the value they would have on some datum equipotential surface such as the geoid, or surface

everywhere parallel to it, some adjustment is important. Since it is not always possible to measure gravity on the geoid, gravity values observed at different topographical environment should be reduced to the geoid equipotential surface by the following important components of gravity data reduction; free air correction, Bouguer correction, Terrain (topographic) correction latitude correction and drift correction.

I. Latitude Corrections: - Correction subtracted from the observed gravity that accounts for Earth's elliptical shape and rotation. Both the rotation of the earth and its slights equatorial bulge produce an increase of gravity with latitude. The centrifugal acceleration due to its spinning earth, maximum at the equator and zero at the poles- opposes the gravitational acceleration while polar flattening also increases gravity at the poles (Telford, 1990). As indicated in chapter two, our study covers very small area which leads us to consider latitude correction insignificant Therefore, this research ignores latitude correction.

II. Free Air Correction: - The free air correction compensates the observed gravity for the fact that it was measured at a given height above (or below) the datum. It assumes, however, that there is nothing but air between the geoid or ellipsoid and the observation point. It also accounts for the changing distance to the Earth center of mass and this is a positive correction when gravity is measured above sea level. This correction is given by the formula;

$$\delta g_f = 0.3086h\, mGal \qquad 3.30$$

where h is the topographic height above sea level.

Note that the free air correction is added to the gravity readings when the station is above the geoid and subtracted when below it.

III. Drift Correction: - The variation of repeated gravimeter reading at the same base station at short duration intervals known as gravimetery drift and is due to non-geologic effects that are presumed to arise from thermal and pressure induced non cyclic gradual changes in the elastic property of the gravimeter. The effect of gravimeter drift is small for modern gravimeters and can be compensated by making a correction known as drift correction.

Note that positive drift requires negative correction and vice versa.

IV. Tidal Correction: - Gravity measured at a fixed location varies with time because of the periodic variation in the gravitational effect of the Sun and the Moon associated with their orbital motion, and correction must be made for this variation in high precision survey. Tidal correction can be calculated from knowledge of locations of the Sun and the Moon as a function of time. Repeated measurement at the same base stations over short time intervals permits the estimation of tidal correction. However, because tidal variations are smooth and relatively too low, tidal correction is usually included in the drift correction.

V. Bouguer Correction: - Surveys are usually conducted on the land surface. As one changes elevation there are changes in g caused by the added (or subtracted) layer of material that has been included. Thus in moving up from a valley to a plateau the gravity decreases due to the increasing distance from the center of mass but is also increased by the attraction of the slab of rock whose thickness is the change in elevation.

The effect of this intervening slab is called the Bouguer effect or Bouguer correction. It is the opposite sign to the free air correction. Since the latitude and free air effects, and to a good approximation the Bouguer effect, are accurately predictable it is common practice to correct the data to a reference level. This essentially removes the large first order variations along the profile and permits the ready identification of the anomaly due to the buried density inhomogeneity or mass deficit in the case of the cave.

The Bouguer correction, derived by assuming the slab to be of infinite horizontal extent is given by:

$$\delta g_B = 2\pi G\rho h \qquad 3.31$$

Where h is the height of the gravity station above the geoid and G is the gravitational constant and ρ is the density of the material for mean crustal density (ρ=2.67gm/cm3) and h in meters, the Bouguer correction reduces to:

$$\delta g_B = 0.0419\rho h\, mGal \qquad 3.32$$

The Bouguer correction is applied in the opposite sense to free- air correction. It is subtracted when the station is above the datum plane and vice-versa.

VI. Terrain Correction: - The Bouguer correction makes the assumption that the topography around the gravity station is flat. This is rarely the case and further correction; the terrain correction must be made to account for topographic relief in the vicinity of the gravity station. The Terrain correction accounts for variations in the observed gravitational acceleration caused by variations in topography near each observation point. Because of the assumptions made during the Bouguer Slab correction, the terrain correction is positive regardless of whether the local topography consists of a mountain or a valley. Terrain corrections are, therefore, always positive and always added to the station reading. There is no simple mathematical formula for the computation of g_t ; however, there are several graphical methods for calculating terrain corrections. All of them require a good topographical map of the area.

3.2.8 Gravity Anomalies

When the Free Air Correction and the Bouguer Correction performed on the observed gravity, the observed gravity g_p reduced to the mean sea level geiod denoted by g_o and is known as Bouguer reduction or simple Bouguer reduction given by;

$$g_o = g_p + \delta g_f - \delta g_B \qquad 3.32$$

The difference between the mean sea level (Geoid) reduced observed gravity g_o and the theoretical gravity γ calculated at the mean sea level Ellipsoid point O is known as simple Bouguer anomaly Δg_B given by;

$$\Delta g_B = g_o - \gamma = g_p + \delta g_f - \delta g_B - \gamma \qquad 3.33$$

After some mathematical computation the simple Bouguer anomaly Δg_B also given by;

$$\Delta g_B = g_p + 0.3086h - 0.0419\rho h - \gamma \qquad 3.34$$

For gravity survey in an area of rugged topography all the correction i.e. the Free Air Correction, the Bouguer Correction and Terrain Correction should be made in order to

reduce the observed gravity to the mean sea level Geiod known as the complete Bouguer reduction and is given by;

$$g_o = g_p + 0.3086h - 0.0419\rho h + \delta g_t \quad 3.35$$

Consequently, the difference between the mean sea level reduced gravity g_o , and the theoretical gravity γ calculated at mean sea level pointO is known as complete Bouguer anomaly and is given by;

$$\Delta g_{CB} = \left(g_p + 0.3086h - 0.0419\rho h + \delta g_t\right) - \gamma \quad 3.36$$

The Bouguer anomaly reflects the subsurface inhomogeneities in density. It should also be noted here that the Bouguer anomaly is caused by the excess mass associated with a volume of density enclosed by a medium of density.

3.3 The Magnetic Method

3.3.1 Introduction

The aim of a magnetic survey is to investigate subsurface geology on the basis of anomalies in the Earth's magnetic field resulting from the magnetic properties of the underlying rocks. Although most rock-forming minerals are effectively non-magnetic, certain rock types contain sufficient magnetic minerals to produce significant magnetic anomalies. Similarly, man-made ferrous objects also generate magnetic anomalies. One of the uses of magnetic survey is identifying and locating tectonic structures (fault, fractures, fissures, contacts, graben) that might act as geothermal fluid circulation channels as well as possible reservoir rocks of high secondary permeability.

Ground magnetic surveys are used in geothermal exploration to map subsurface structural features and as an aid to geological mapping where outcrops are scarce. The purpose of magnetic surveys is to detect rocks or minerals possessing contrasting magnetic properties, which revel themselves by causing disturbances or anomalies in the intensity of the Earth's magnetic field. In some high-temperature geothermal areas, a good correlation is found between altered ground and the reduced intensity of magnetization caused by the alteration of magnetic minerals (Palmasson, 1975).

In geothermal application the main objective of the magnetic study is to contribute with information about the relationship among the geothermal activity, the tectonic and stratigraphy of the area by means of the anomalies interpretation of the underground rocks' magnetic properties (Escobar, 2005). Most of the rocks are not magnetic; however, certain types of rocks contain enough minerals to originate significant magnetic anomalies. The data interpretation that reflects differences in local abundance of magnetization is especially useful to locate faults and geologic contacts (Blakely, 1995).

Although magnetic and gravity methods are the two potential methods that have some properties in common, there are some basic differences between this two methods. One example of all these is that precise interpretation of magnetic field data is much more complex than for gravity.

3.3.2 Principles and Elementary Theory

If two magnetic poles of strength m_1 and m_2 are separated by a distance r, a force, F, exists between them. If the poles are of the same polarity, the force will push the poles apart, and if they are of opposite polarity, the force is attractive and will draw the poles together. In general, the magnetic force f (attraction or repulsion force) acting between two magnetic poles of strengths m_1 and m_2 separated by a distance r is determined by Coulomb's law given by:

$$f = \frac{-\mu_o}{4\pi\mu_r}\frac{m_1 m_2}{r^2} \qquad 3.37$$

Where μ_o is the magnetic permeability of the vacuum and μ_r is relative magnetic permeability of the medium separating the poles; m_1 and m_2 are pole strengths and r the distance between them.

The *magnetic field strength*, H, is defined as the force per unit pole strength exerted by a magnetic monopole, m_1. H is nothing more than Coulomb's expression divided by m_2. The magnetic field strength H is the magnetic analog to the gravitational acceleration, g.

$$H = \frac{-\mu_O}{4\pi\mu_r}\frac{m_1}{r^2} \qquad 3.38$$

Given the units associated with force, *N*, and magnetic monopoles, Amp-m, the units associated with magnetic field strength are Newton per Ampere-meter, N / (Amp- m*)*. (Amp - m) is referred to as a tesla (T), named after the renowned inventor Nikola Tesla.

The magnetic flux lines between two poles per unit area, is the flux density H (and is measured in weber/m^2 = Tesla).H, which is also called the "magnetic induction", is a vector quantity. The unit of Tesla are too large to be practical in geophysical work, so a sub-unit called a nanotesla (1 nT = 10^{-9} T) is used instead, where 1 nT is numerically equivalent to 1 gamma in c.g.s. units (1 nT is equivalent to 10^{-5} gauss). The magnetic field can also be defined in terms of a force field which is produced by electric currents. This magnetizing field strength **H** is defined, following Biot-Savart's Law, as being the field strength at the centre of a loop of wire of radius r through which a current I is flowing such that $H = I/2r$**.**

Consequently the units of the magnetizing field strength **H** are amperes per meter (A/m). The ratio of the flux density **B** to the magnetizing field strength **H** is a constant called the absolute magnetic permeability (μ).

The concept of a magnetic dipole is basic for an understanding of the magnetic behavior of matter ranging in dimensions from small magnetic particles to the entire Earth. Mathematically we consider a dipole to consisting of two magnetic poles strength, -*m* and +*m* separated by a finite distance *d*. therefore, the magnetic moment is defined as:

$$M = md \tag{3.39}$$

Where, M is the magnetic moment or dipole moment.

When a magnetic material, say iron, is placed within a magnetic field, *H*, the magnetic material will produce its own magnetization. This phenomenon is called *induced magnetization*. The intensity of magnetization is proportional to the strength of the field and its direction is in the direction of that field.

It is defined as the magnetic moment per unit volume, that is,

$$J_i = \frac{M}{V} \tag{3.40}$$

where, J_i is the induced polarization or induced magnetization.

The intensity of magnetization, J_i, is related to the strength of the inducing Magnetic field, *H*, through a constant of proportionality, k, known as the Magnetic Susceptibility.

$$J_i = KH \tag{3.41}$$

The magnetic susceptibility is a unit less constant that is determined by the physical properties of the magnetic material. It can take on either positive or negative values. Positive values imply that the induced magnetic field, J_i, is in the same direction as the inducing field, *H*. Negative values imply that the induced magnetic field is in the opposite direction as the inducing field.

In magnetic prospecting, the susceptibility is the fundamental material property whose spatial distribution we are attempting to determine. In this sense, magnetic susceptibility is analogous to density in gravity surveying.

In vacuum the magnetic field, B, strength and magnetizing force, H, is related by:

$$B = \mu_O H \tag{3.42}$$

μ_O – The permeability of the vacuum ($4\pi \times 10^{-7} Hm^{-1}$).

The total magnetic field (induction) B in a body placed in a magnetic field is given by:

$$B = \mu_o H + \mu_o J_i \tag{3.43(a)}$$

$$B = \mu_o H + \mu_o kH \tag{3.43(b)}$$

$$B = (1 + k)\mu_o H \tag{3.43(c)}$$

$$B = \mu_o \mu_r H \tag{3.43(d)}$$

where μ_r is a dimensionless constant known as the relative magnetic permeability.

So magnetic permeability μ is given by:

$$\mu = \mu_o \mu_r \tag{3.44}$$

The permeability is a measure of the modification by induction of the force of attraction or repulsion between two magnetic poles. Its magnitude depends on the magnetic properties of the medium in which the poles are immersed.

3.3.3 Magnetism of the Earth

Ninety percent of the Earth's magnetic field looks like a magnetic field that would be generated from a dipolar magnetic source located at the center of the Earth and aligned with the Earth's rotational axis. Sir William Gilbert first gave this first order description of the Earth's magnetic field in 1600. The strength of the magnetic field at the poles is about 60,000 nT. If this dipolar description of the field were complete, then the magnetic equator would correspond to the Earth's equator and the magnetic poles would correspond to the geographic poles. As we've come to expect from magnetism, such a simple description is not sufficient for analysis of the Earth's magnetic field. The remaining10% of the magnetic field cannot be explained in terms of simple dipolar sources. Complex models of the Earth's magnetic field have been developed and are available.

I) The geomagnetic field (Main field)

The causes of the geomagnetic field is attributed to a dynamo action produced by the circulation of charged particles in coupled convictive cells within the outer fluid parts of the Earth's core, the major constituent is liquid iron for the generation of the main field, and the important parameters of the core are its, temperature, viscosity and electrical conductivity.

A) Elements of earth's magnetic field.

A vector is used to represent the Earth's magnetic field at an observation site. The vector is described by a combination of seven quantities known as the magnetic elements (Fig. 3.4). The total field vector B has a vertical component Z and a horizontal component H in the direction of the magnetic north. Inclination I is the angle between the directions of the B-field and the horizontal plane. Magnetic declination D is the horizontal angle between the geographic north and the magnetic north that is indicated by a compass. The horizontal

component H can be further decomposed into a component X in the geographical north direction and a component Y in the geographical east direction.

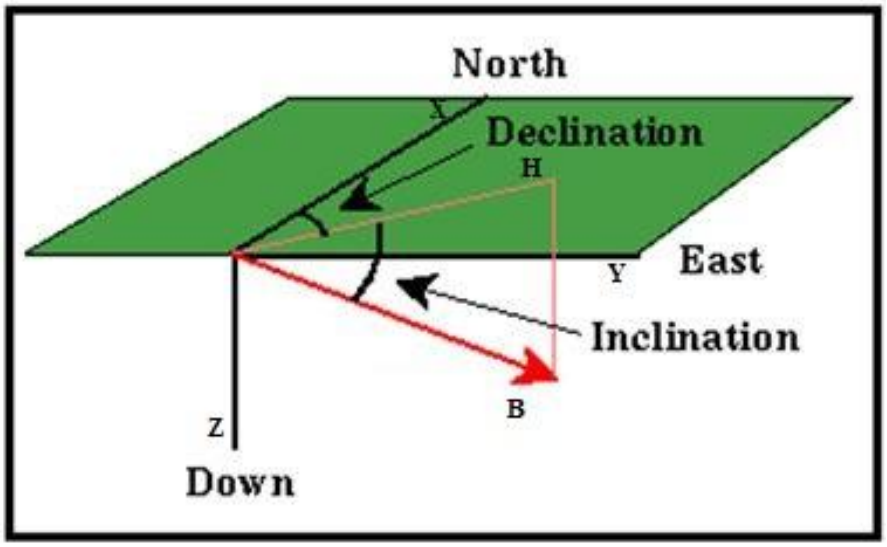

Figure 3.4 Elements of Earth's magnetic field.

The seven Earth's magnetic field elements are related by the following relations:

$$X = H\cos D \qquad Y = H\sin D \qquad H = \sqrt{X^2 + Y^2} \qquad 3.45$$

$$H = B\cos I \qquad Z = B\sin I \qquad B = \sqrt{H^2 + Z^2} = \sqrt{X^2 + Y^2 + Z^2}$$

Where, H, Z, D magnetic elements recorded at geomagnetic observatories.

Any combination of three magnetic elements is sufficient to completely describe the Earth's magnetic field vector at an observation site.

B) Secular Variations

The circulation pattern within the core is not fixed and change slowly with time, the temporal change in the geomagnetic elements known as secular variation. Secular variation of the internal geomagnetic field originates in the upper part of the fluid outer core; it consists of fluctuations in intensity and direction with periods of the order 10-10^4yr. Paleomagnetic

observations show that, there is also the periodic change in geomagnetic field polarity due to the change in circulation pattern within the outer fluid parts of the Earth's core.

II) The External Magnetic Field

Most of the very short wave length fraction of the solar radiation does not reach the Earth's surface. Energetic γ-ray and x-ray and UV-radiations causes' ionization of molecules of N_2 and O_2 in the thin upper atmosphere in altitude between 50km-1500km forming an ionized region called the **ionosphere.** Electric current in the ionosphere arise from systematic motion of the ions, which are affected by different factors such as, the daily and monthly tides and the periodic fluctuation in ionization related to the 11yr sunspot cycle, thus the current induce varying magnetic field which is associated with the external origin of Earth's magnetic field.

A) Diurnal variations

Magnetic effects of the external origin causes the geomagnetic field to vary on a daily bases to produce diurnal variations. Such variation results from the magnetic field induced by the flow of charged particles within the ionosphere to ward magnetic poles, as both the circulation patterns and diurnal variations vary in sympathy with the tidal effects of the sun and the moon. As the Earth rotate beneath the ionosphere the observed intensity of the geomagnetic field fluctuate with a range of amplitude of about 10-30nT at the Earth's surface within a period of one day this variation in geomagnetic field intensity is known as diurnal (daily) variation.

B) Magnetic storm

The enhance emission of radiation associated with the solar phenomena increase the ionosphere current, this give raise to rapid varying anomalously strong magnetic field. Some days (disturbed days) are distinguished by far less regular diurnal variations and involve large short term disturbance in the geomagnetic field with amplitude of up to 1000nT, known as magnetic storm, during this period magnetic survey should be ceased.

III) Magnetic anomalies

A magnetic anomaly originates from the susceptibility contrasts between susceptibility of anomalous rock body and the susceptibility of the surrounding rock. The shape of magnetic anomaly depends not only on the shape and depth of the anomalous body but also on its orientation with respect to the direction of the profile considered and with respect to the direction of the inducing magnetic field, which itself varies in intensity and direction with respect to its geographical locations. The susceptibility contrast is due to induced magnetization J_i of crustal rocks.

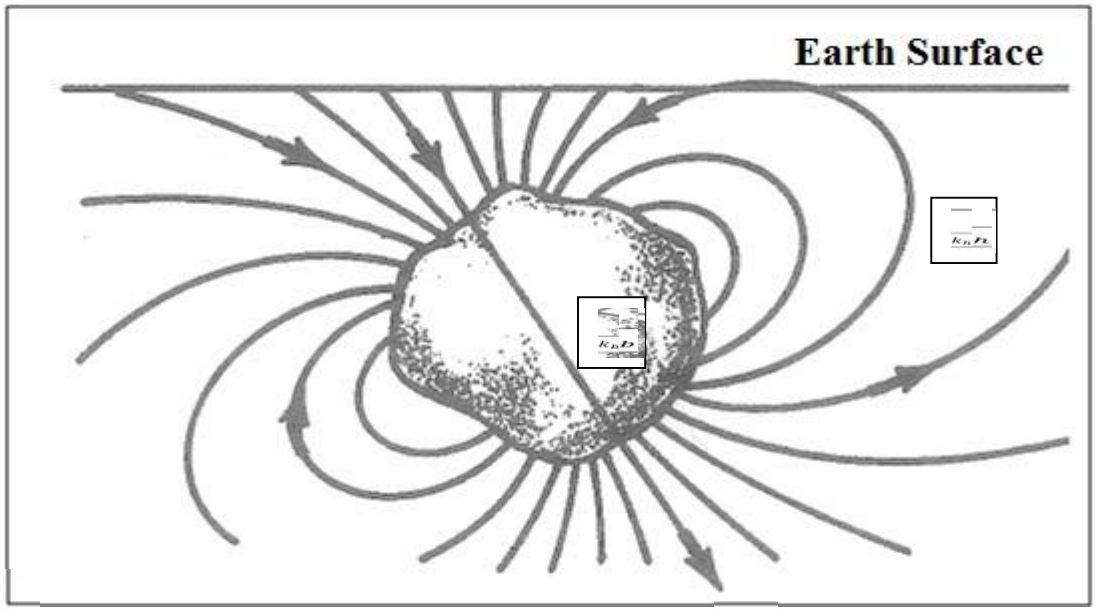

Figure 3.5 an ore body behaves like a huge buried magnet (taken from Buriner, 1999)

If k_b represent the susceptibility of an anomalous body and k_h is the susceptibility of the host rocks, the susceptibility contrasts Δk is given by:

$$\Delta k = k_b - k_h \qquad 3.46$$

$\Delta k > 0$, results in positive magnetic anomaly and $\Delta k < 0$, results in negative magnetic anomaly.

3.3.4 Magnetic Data Reduction

Measurements (magnetic, gravity etc) are normally made at a regular or random intervals along a grid or otherwise selected paths whose locations are noted for subsequent plotting.

Corrections (diurnal correction,δB) are applied to the measured values (B_{obs}). The dipole field determined from International Geomagnetic Reference Field (IGRF) maps is subtracted from the measurements acquired at each station to generate magnetic anomalies as:

$$\Delta B = B_{obs} \pm \delta B - B_D \qquad 3.47$$

The most significant correction is for the diurnal variation in the Earth's magnetic field. The necessary corrections are mostly attempted by the reoccupation of the base station which is located in or near the survey area.

3.5 The Electrical Resistivity Method

3.5.1 Introduction

Surface electrical resistivity surveying is based on the principle that the distribution of electrical potential in the ground around a current-carrying electrode depends on the electrical resistivity and distribution of the surrounding soils and rocks. The usual practice in the field is to apply an electrical direct current (DC) between two electrodes implanted in the ground and to measure the difference of potential between two additional electrodes that do not carry current. Usually, the potential electrodes are in line between the current electrodes, but in principle, they can be located anywhere. The current used is either direct current, commutated direct current (i.e., a square-wave alternating current), or AC of low frequency (typically about 20 Hz). All analysis and interpretation are done on the basis of direct currents. The distribution of potential can be related theoretically to ground resistivity's and their distribution for some simple cases, notably, the case of a horizontally stratified ground and the case of homogeneous masses separated by vertical planes (e.g., a vertical fault with a large throw or a vertical dike). For other kinds of resistivity distributions, interpretation is usually done by qualitative comparison of observed response with that of idealized hypothetical models or on the basis of empirical methods.

In electrical resistivity method, a direct, accumulated or low frequency alternating current is introduced into the ground by means of two electrodes; while potential between two points on the ground is measured by other two point electrodes called potential electrodes. The sub-

surface rock resistivity variations affect the electrical current flow that affects the distribution of surface rock resistivity variations affects the distribution of the surface electrical potential. Deviation from the pattern of potential difference expected from a homogeneous ground provides information on the form of the subsurface anomalous mass that is referred to as resistivity anomaly (Parasnis, 1989).

3.5.2 Fundamental Principles of the Method

Measurements of electrical resistivity are made with circuits in which the earth is one of the components, namely, a resistor. The physical principle underlying the electrical resistivity method is embodied in Ohm's law. Assuming a continuous current flowing in an isotropic homogeneous medium, if ΔA is an element of surface and J the current density, then the current passing through ΔA is $J\Delta A$. The current density J and the electrical field E are related through Ohm's law as:

$$J = \delta E \tag{3.48}$$

Where, E is in volts/meter and δ is the conductivity of the medium in mhos/meter.
The electric field is a negative gradient of electric potential, which is a scalar physical quantity and given by the equation:

$$E = -\nabla V \tag{3.49}$$

Where, V is in volts.
After substituting equation (3.49) into equation (3.48), the equation is given by:

$$J = -\delta \nabla V \tag{3.50}$$

If the medium is homogeneous, the electrical potential distribution for direct current, in a homogeneous medium, satisfies the **Laplace equation**, the equation that which is obtained after considering some necessary conditions, and is given by:

$$\nabla^2 V = 0 \tag{3.51}$$

Mostly two electrodes are used to supply a controlled electrical current to the ground. Such electrodes are called current electrodes. From the two current electrodes, there is a set of successive equipotential surfaces, in the form of a hemispherical surface. The potential difference between the equipotential surfaces can be measured where they intersect the ground surface using a second pair of electrodes called potential electrodes. Consider an electrode of small dimensions buried in a homogeneous isotropic medium. The current circuit is completed through another electrode, usually at the surface placed at infinite distance or at least at far distance so that its effect is negligible.

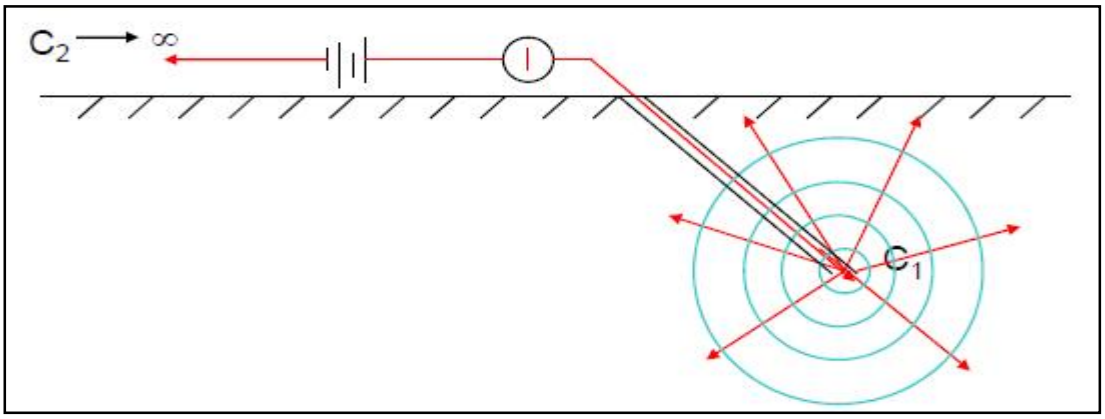

Figure 3.6 Buried point source of current in a homogeneous ground (Dr. Tigstu Haile, 2006).

As shown in the above figure, the current lines will be directed radially outwards from the source. From the symmetry of the problem, the potential will be a function of only the radial distance 'r' from the source electrode. Under this conditions Laplace's equation, in spherical coordinates, simplifies to:

$$\nabla^2 V = \frac{\partial^2 V}{\partial r^2} + \frac{2}{r}\frac{\partial V}{\partial r} = 0 \qquad 3.52$$

When the above equation is multiplying throughout by r^2, it takes the form given by:

$$r^2 \frac{\partial^2 V}{\partial r^2} + 2r\frac{\partial V}{\partial r} = 0 \qquad 3.53$$

Integrating both sides of the equation,

$$\int r^2 \frac{\partial^2 V}{\partial r^2} + 2r \frac{\partial V}{\partial r} \partial r = 0 \qquad 3.54$$

This implies that;

$$\frac{\partial V}{\partial r} = \frac{-A}{r^2} \qquad 3.55$$

Integrating equation (3.55) once more;

$$V = \frac{-A}{r} + B \qquad 3.56$$

where A and B are integration constants.

Boundary conditions

1. Since V=0 as r → ∞, this implies that B=0
2. the total current flowing through a sphere of radius r, hence

$$I = 4\pi r^2 \vec{J}, \qquad \vec{J} = -\delta \vec{E} = -\delta \frac{\partial V}{\partial r} = -\delta \frac{A}{r^2}$$

$$= 4\pi r^2 \left(-\delta \frac{A}{r^2}\right)$$

Hence;

$$I = -4\pi\delta A \rightarrow A = \frac{-I\rho}{4\pi}$$

where $\delta = \frac{1}{\rho}$ is the resistivity of the homogeneous layer.

So that in this case,

$$V = \frac{I\rho}{4\pi}\left(\frac{1}{r}\right) \; or \; \rho = 4\pi r \left(\frac{V}{I}\right) \qquad 3.57$$

Considering the case where the current electrode is located at the surface of a fictitious homogeneous earth and now all the current flows through hemispherical surface in the lower half only because of the air above the electrode has zero conductivity, Equation (3.57) takes the form:

$$V = \frac{I\rho}{2\pi}\left(\frac{1}{r}\right) \; or \; \rho = 2\pi r\left(\frac{V}{I}\right) \qquad 3.58$$

This leads to the formula for the ground resistivity to any electrode configuration.
The electrical resistivity of the ground as measured by two potential electrodes after current is introduced to the ground by two other current electrodes is:

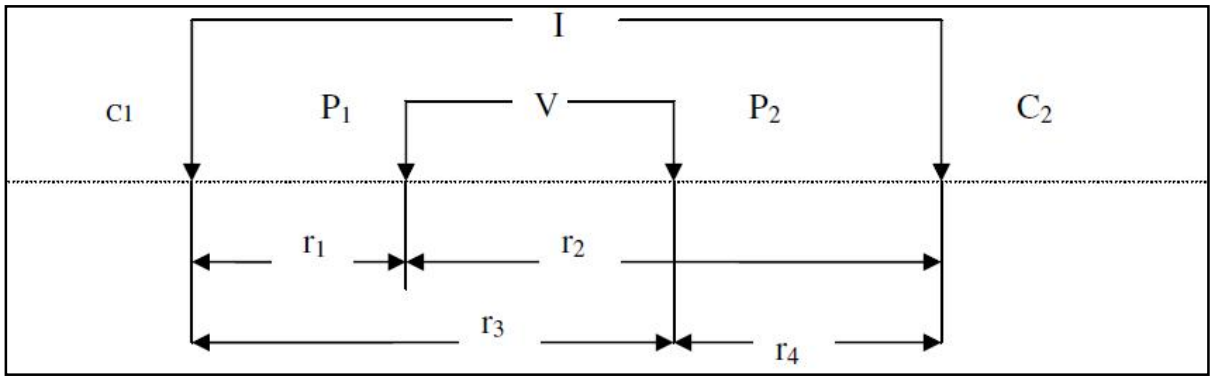

Figure 3.7 Two current and two potential electrodes on the surface of homogenous isotropic ground of resistivity ρ (Telford, 1990).

From the diagram electrical resistivity of the ground surface can be derived as:
The potential at point P1 is;

$$V_{P1} = \frac{I\rho}{2\pi}\left[\frac{1}{r_1} - \frac{1}{r_2}\right] \qquad 3.59$$

And the potential at P2 is;

$$V_{P2} = \frac{I\rho}{2\pi}\left[\frac{1}{r_3} - \frac{1}{r_4}\right] \qquad 3.60$$

The potential difference between P_1 and P_2, ΔV will be:

$$\Delta V = V_{P1} - V_{P2}$$

$$\Delta V = \frac{I\rho}{2\pi}\left[\left(\frac{1}{r_1} - \frac{1}{r_2}\right) - \left(\frac{1}{r_3} - \frac{1}{r_4}\right)\right] \quad 3.61$$

Or

$$\rho = \left\{\frac{1}{\frac{1}{r_1} - \frac{1}{r_2} - \frac{1}{r_3} + \frac{1}{r_4}}\right\}\left(\frac{\Delta V}{I}\right) \quad 3.62$$

$$\rho = K\left(\frac{\Delta V}{I}\right) \quad 3.63$$

where K is the geometric factor

Wherever these measurements are made over a real heterogeneous Earth, as distinguished from the fictitious homogeneous half-space, the symbol ρ is replaced by ρ_a for apparent resistivity. The resistivity surveying problem is, reduced to its essence, the use of apparent resistivity values from field observations at various locations and with various electrode configurations to estimate the true resistivity of the several earth materials present at a site and to locate their boundaries spatially below the surface of the site.

The resistivity determined would have been true resistivity if the ground were homogeneous and isotropic. However, usually the ground constitutes various materials and there might be some variations in the lateral or vertical dimensions and the resistivity determined is called apparent resistivity. The apparent resistivity measured depends not only on the nature of the geologic formation but also on the geometric dispositions. And hence Equation (3.63) will be modified as:

$$\rho_a = K\left(\frac{\Delta V}{I}\right) \qquad 3.64$$

where ρ_a is the apparent resistivity.

An electrode array with constant spacing is used to investigate lateral changes in apparent resistivity reflecting lateral geologic variability or localized anomalous features. To investigate changes in resistivity with depth, the size of the electrode array is varied. The apparent resistivity is affected by material at increasingly greater depths as the electrode spacing is increased. Because of this effect, a plot of apparent resistivity against electrode spacing can be used to indicate vertical variations in resistivity.

There are several styles of electrode arrangements for resistivity survey, the types of electrode arrays that are most commonly used (Schlumberger, Wenner, and dipole-dipole) are illustrated in figure below.

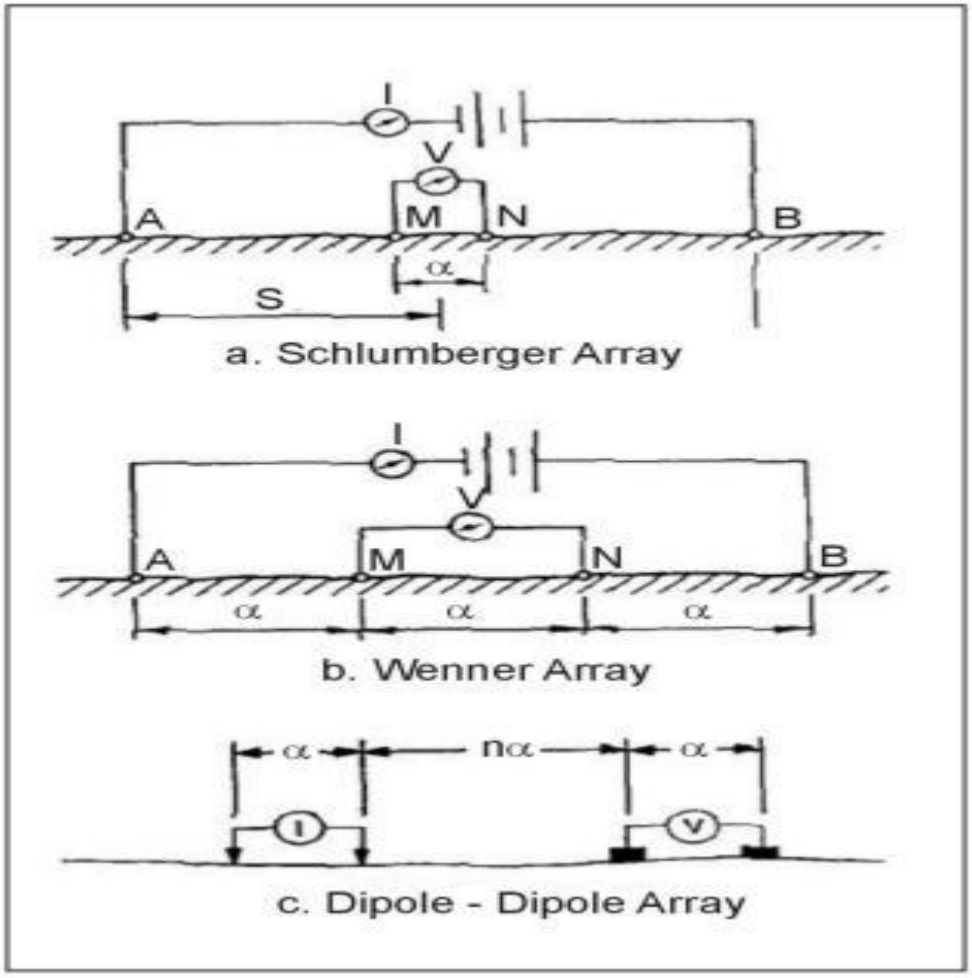

Figure 3.8 Schlumberger, Wenner, and dipole-dipole electrode arrangements

3.5.3 The Schlumberger Array

The Schlumberger array is the symmetrical arrangement in which the points A,M,N and B are taken on a straight line such that the points are symmetrically taken about the center of the spread (sounding point),O. When this arrangement is used for sounding, the separation is kept constant for a number of AB values, which are successively increased for larger depth penetrations. Nevertheless, when the value of MN, in comparison to AB, becomes too small the potential difference drops significantly, to be measured precisely, it needs to be increased accordingly.

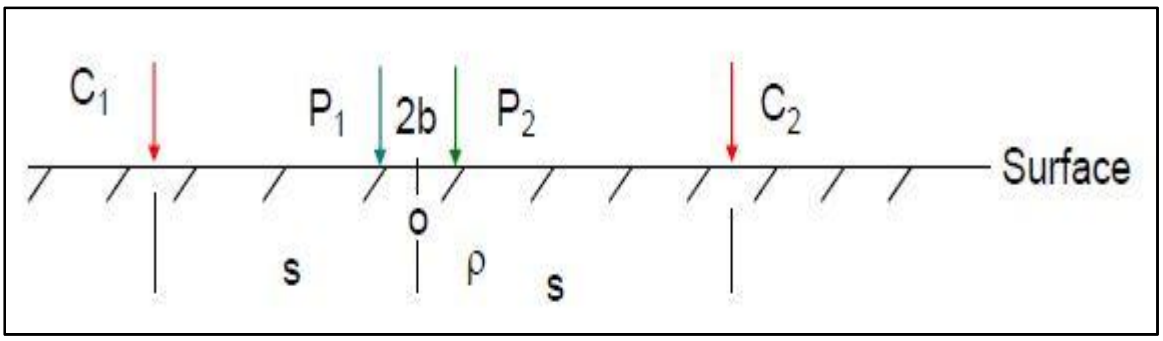

Figure 3.9 Electrode spreads in Schlumberger array (Dr. Tigstu Haile, 2006)

From the above one can observe the following relations.

$$r_1 = s - b,\ r_2 = s + b, r_3 = s + b, r_4 = s - b$$

Substituting the above relations in to equation (3.61) and operating the mathematical relations;

$$\Delta V = \frac{I\rho}{2\pi}\left(\frac{2b}{s^2-b^2}\right) \qquad 3.65$$

Or

$$\rho_{ascu} = \pi\left[\frac{s^2-b^2}{2b}\right]\left(\frac{\Delta V}{I}\right) \qquad 3.66$$

where, ρ_{asuh} is apparent resistivity in Schlumberger array.

$\pi\left(\frac{s^2-b^2}{2b}\right)$ - is the geometric factor in the Schlumberger array.

Either the Schlumberger or, less effectively, the Wenner array is used for sounding, since all commonly available interpretation methods and interpretation aids for sounding are based on these two arrays. In the use of either method, the center point of the array is kept at a fixed location, while the electrode locations are varied around it. The apparent resistivity values, and layer depths interpreted from them, are referred to the center point.

By virtue of its relative advantage over other arrays, the electrode configurations widely used in sounding is that of Schlumberger array. In the Schlumberger sounding, the values of MN and the corresponding AB values are chosen in order to get overlapping readings whenever a change over MN values takes place.

3.5.4 Field Procedure in Electrical Resistivity Method

Regardless of the specific electrode spread employed, there are only two basic procedures in resistivity work. The particular procedure to be used depends on whether one is interested in resistivity variations with depth or with lateral extent. These two procedures are known as electrical drilling or vertical electrical sounding (VES), electrical profiling, or mapping or sometimes known as lateral inhomogeneity hunter.

I. Vertical Electrical Sounding (VES)

In VES, a set of measurements are taken, at a specific point, such that the value of K is progressively changed resulting in values reflecting the vertical stratification of resistivity in the sub surface, beneath the point of observation. That is why VES is sometimes known as "vertical electrical drilling". VES surveys with the Schlumberger array are also made with a fixed center point, minimum and maximum spacing's are governed by the need to define the asymptotic phases of the apparent resistivity curve and the needed depth of investigation. An initial spacing s (the distance from the center of the array to either of the current electrodes) is chosen, and the current electrodes are moved outward with the potential electrodes fixed.

II. Electrical Resistivity Profiling

Field data may be plotted in the form of profiles or as contours on a map of the surveyed area. For a contour map, resistivity data obtained at grid points are preferable to those obtained from profile lines, unless the lines are closely spaced, because the alignment of data along profiles tends to distort the contour map and gives it an artificial grain that is distracting and interferes with interpretation of the map. The best method of data collection

for a contour map is to use a square grid, or at least a set of stations with uniform coverage of the area, and without directional bias.

Occasionally, a combination of vertical and horizontal methods may be used. Where mapping of the depth to bedrock is desired, a vertical sounding may be done at each of a set of grid points. However, before a commitment is made to a comprehensive survey of this type, the results of resistivity surveys at a few stations should be compared with the drill hole logs. If the comparison indicates that reliable quantitative interpretation of the resistivity can be made, the survey can be extended over the area of interest.

When profiling is done with the Wenner array, it is convenient to use spacing between stations equal to the electrode spacing, if this is compatible with the spacing requirements of the problem and the site conditions. In moving the array, the rearmost electrode need only be moved a step ahead of the forward electrode, by a distance equal to the electrode spacing. The cables are then reconnected to the proper electrodes, and the next reading is made. With the Schlumberger array, however, the whole set of electrodes must be moved between stations.

CHAPTER FOUR

4. DATA ACQUISITION, PROCESSING, PRESENTATION AND INTERPRETATION

4.1. Data point locations

One of the objective of this research work involved obtaining secondary gravity and electrical resistivity data from an available source, executing field work to acquire an original magnetic data and achieve the required magnetic data acquisition skills in the process, hence about 200 gravity and 56 electrical (VES) data employed in this study are obtained from the Geological Survey of Ethiopia (GSE), department of geophysics. Near about 200 primary magnetic data are utilized in this research work. Figure (4.1), Location of Gravity, Magnetic and Electrical data points are plotted using Google Earth satellite image and ArcGis… software.

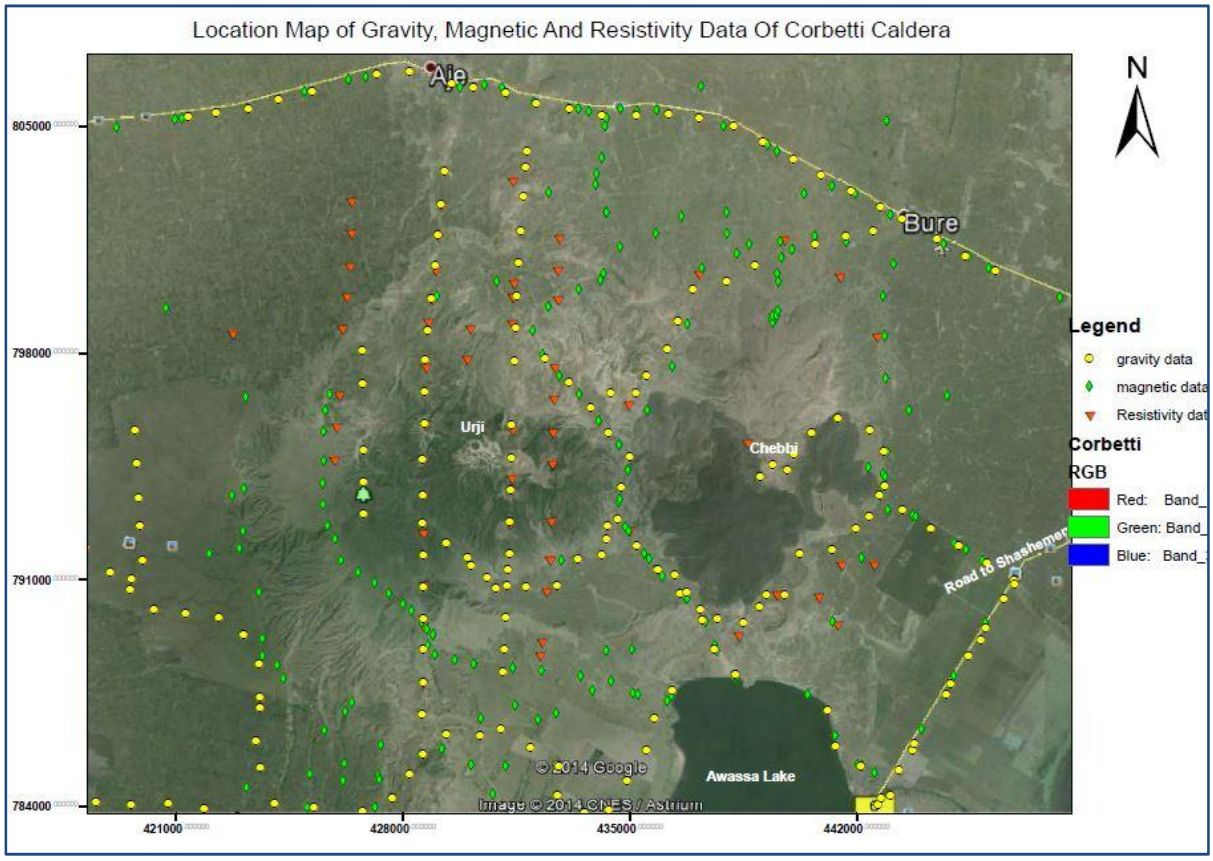

Figure 4.1 Location plots of Gravity, Magnetic and Electrical data point.

4.2. The Gravity Method

4.2.1 Acquisition and Processing of the Gravimetric Data

The gravity data employed in this study are obtained from the Geological Survey of Ethiopia (GSE), department of geophysics and the instrument which is used to collect the data is Lacoste & Romberg gravimeter.

The theoretical gravity, g at latitude ϕ, has been calculated using the 1967 gravity formula (Geodetic reference system 1967; Moritz, 1971). A total of 200 observations are employed for this thesis project and were treated by a homogeneous reference to the IGSN 71 datum. Positions (latitude and longitude) and elevations of the gravity stations are determined by GPS (Global Positioning System) and altimeter measurements.

The Free-air and Bouguer corrections were applied according to the theoretical schemes discussed in the previous sections. A uniform reduction density of 2.67g/cm^3 is used to compute the Bouguer anomalies. The computed Bouguer anomaly corresponds to complete Bouguer anomaly for all stations Therefore, it is the complete Bouguer anomaly that has been considered in this work.

Map presentation and processing, including the preparation of upward continued map from the complete Bouguer anomaly map, and separation of residual components from regional performed by reducing (removing) upward continued map from the regional gravity anomaly map using Geosoft (Oasis Montaj) soft ware.

The end result of the gravity work in the present study is a compilation of regional gravity anomaly maps that includes the area of interest, using the point gravity anomaly values computed at each observation points and preparation of 2D-gravity model constrained with 2D-magnetic model and uses these results to obtain geological picture of the area under investigation. The computed free-air anomaly values are plotted side by side to the point elevation of each station and presented as surface image map. The upward continued gravity map, the complete Bouguer gravity anomaly map and also the residual gravity anomaly map that shows local gravity anomaly are plotted as shown in the preceding pages.

4.2.1.1 Free-Air Gravity Anomaly and Topographic Map

The free air anomaly map Figure (4.2b) shows a strong correlation with local topographic map Fig (4.2a), as shown in the Figure (4.2b), The Free-air anomaly map shows its maximum, about 45mgal and its minimum -2mgal in the study area of interest, i.e., the Chebbi and Urji volcanoes are the highest elevated areas of Corbetti caldera which is about 2100m a above msl and the volcanoes are associated with maximum Free-air anomaly which is about 45mgal.

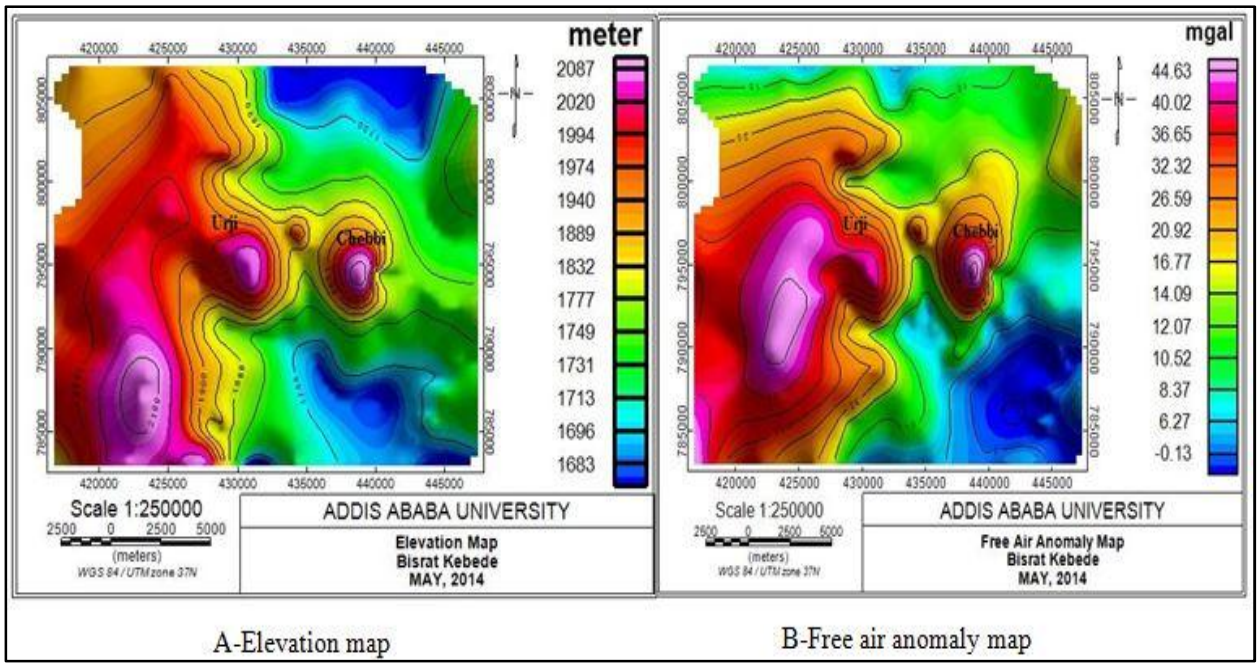

Figure 4.2 Topographic maps (A) and Free-Air anomaly (B) of the Corbetti Caldera and its surroundings

The corresponding region on the topographic map Figure (4.2a) is delineated as higher elevation about between (1900-2100) meters which is associated with the central parts of the caldera and lower elevation values of (1600-1750) meters associated with the local depressions lying on the eastern parts of the elevation map.

4.2.1.2 The Complete Bouguer Gravity Anomaly Map.

The main end-product of gravity data reduction is the Bouguer anomaly, which should correlate only with lateral variations in density of the upper crust and which is of most interest to applied geophysicist and geologists.

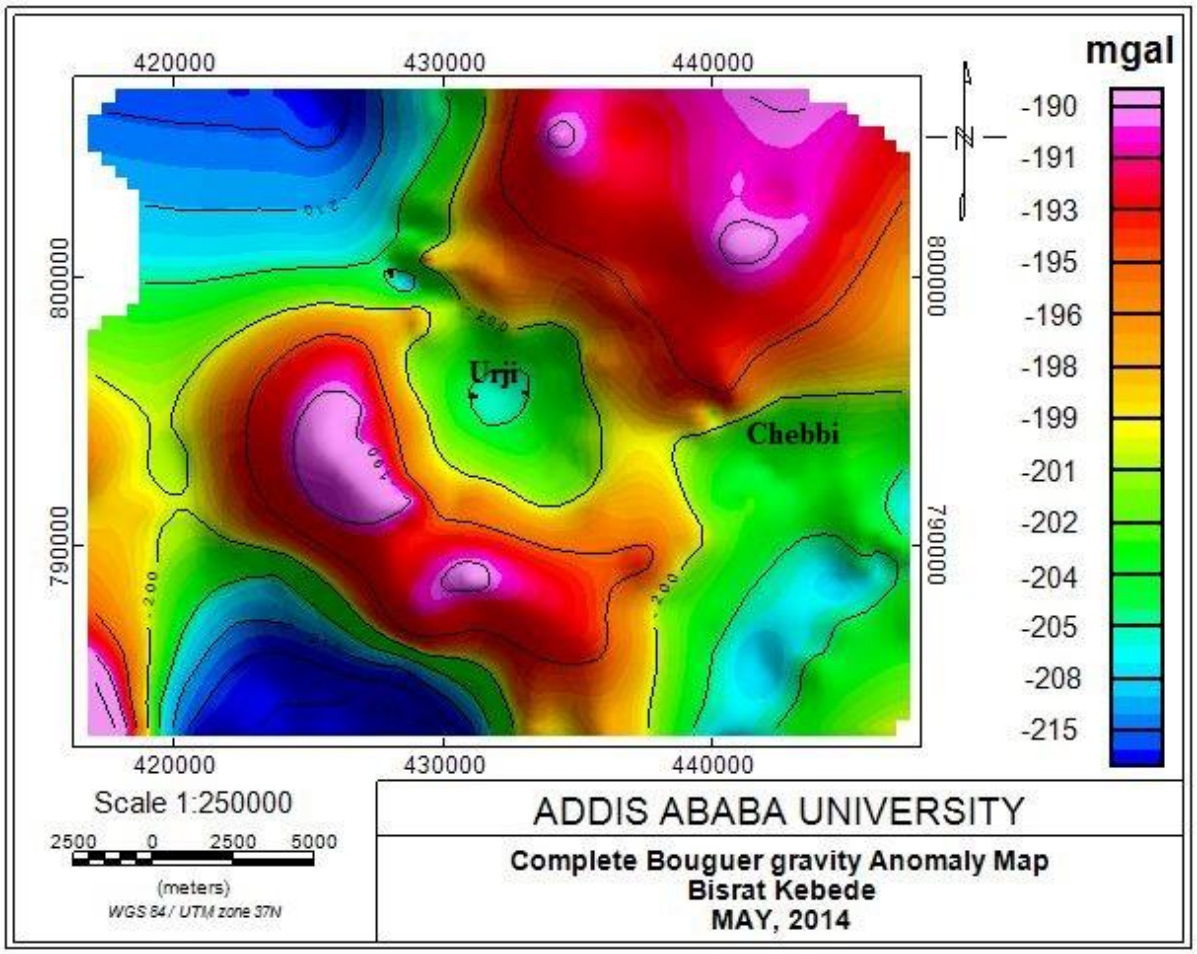

Figure 4.3 Complete Bouguer anomaly map of the Corbetti Caldera and its surroundings.

Referring to the complete Bouguer gravity anomaly map Figure (4.3), which is correlate with lateral variations in density of the upper crust beneath the study area. Generally, the magnitude of the Bouguer gravity anomaly values beneath the study area varies from minimum of -217 mgal to the maximum of -190mgal. Moreover, the anomaly map shows different contrasting anomalous zones (for example, a circular low of about -200 mgal having a steep gradient located at the center of the anomaly map) has outlined the geologically inferred Corbetti caldera.

The minimum gravity anomaly observed over the Chebbi and Urji volcanoes may be due to the reflections of the maximum elevations of the Chebbi and Urji volcanoes as compared to the anomalous zones observed over the rest of the Corbetti caldera and its surroundings.

Observing to the complete Bouguer gravity anomaly map Figure (4.3), the gravity anomaly acquires a maximum value to the NE and SW of the Corbetti caldera. The NE part of the caldera generally coincides with a high gravity anomaly value of (-192mgal to -187mgal) and the SE part which appears like a curve running from SE to NW below the caldera coincides with a high gravity anomaly value of (-193mgal to -190mgal). This gravity highs may be interpreted as the effect the high density materials coming from the mantle during the formation of the caldera. The Southwestern and north western parts of the Corbetti caldera coincide with a minimum value of gravity anomaly (-207mgal to -217mgal) as shown in the complete Bouguer anomaly map. These gravity minima may be interpreted as the effect of low density crust materials.

In general the Corbetti caldera is associated with a high gravity field with slight modifications imposed by the effect of the Chebbi and Urji volcanoes which are relatively associated with low gravity field in the study area. This is due to the fact that the Corbetti caldera consists of mantle derived materials of denser intrusions which come closer to the surface during the volcanic activities.

4.2.1.3 Upward Continued Gravity Anomaly Map

The upward continued gravity anomaly map Figure (4.4) is prepared using GM-SYS-3D model from the complete Bouguer gravity anomaly map by Geosoft Ware Oasis Montaj. The upward continued gravity anomaly map reflects the gravity anomaly of crustal masses buried at approximate depths varying from 15km up to the Mho depth.

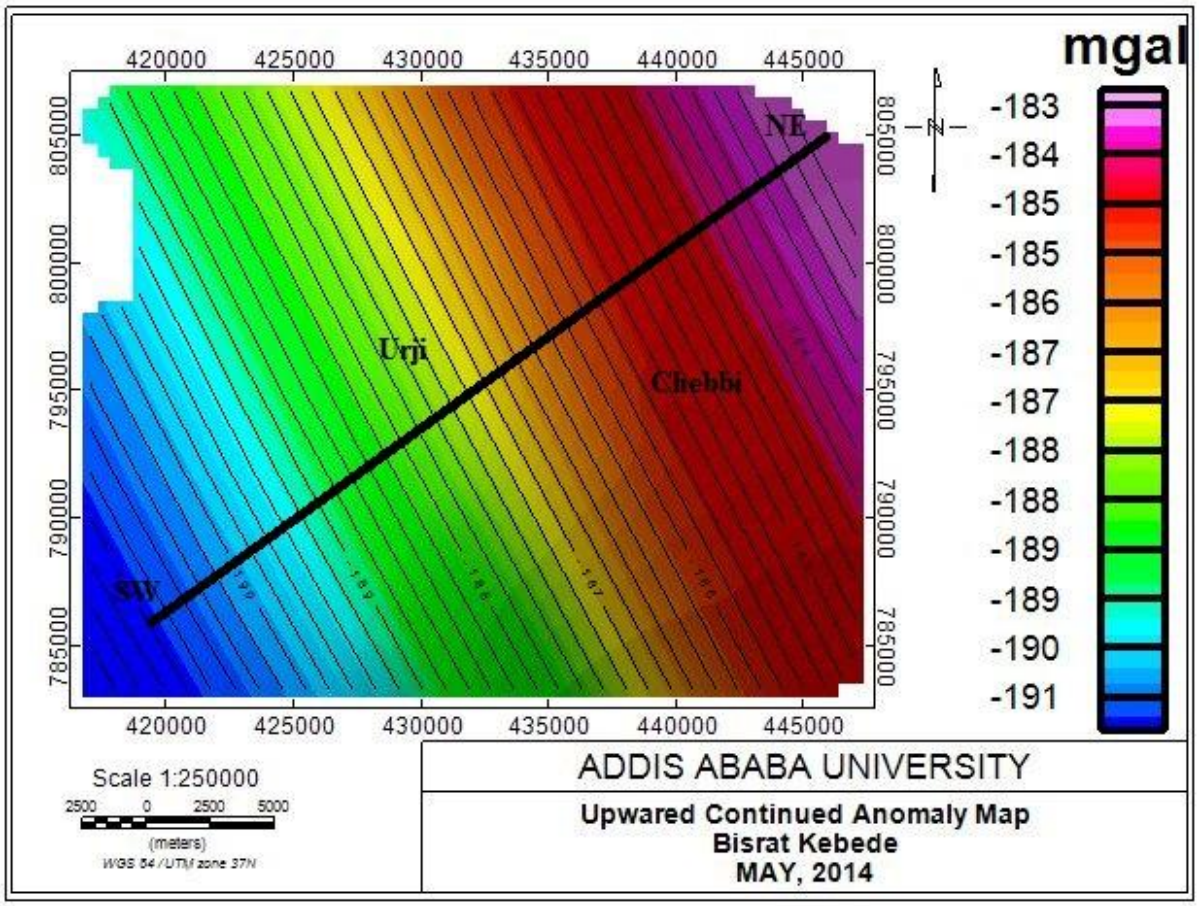

Figure 4.4 Upward continued gravity anomaly map of the Corbetti Caldera and its surroundings.

Referring to the upward continued gravity anomaly map Figure (4.4), the anomaly values contentiously increase as one goes from the southwestern to the northeastern part the study area. The upward continued gravity anomaly map shows the gravity anomaly of deep origin. The continuous gravity anomaly increment without interruption from SW to NE towards the axial portion of the Main Ethiopia Rift (MER) may be interpreted as being caused by the decrease of the crustal thickness of the region along the axial portion of the Main Ethiopia Rift (MER). Along the axial portion of the MER, denser mantle materials approaching closer to the surface has an enormous effect on the gravity field generated beneath the study area.

4.2.1.4 Bouguer Residual Gravity Anomaly Map

Usually it is very difficult to recognize the gravity effect of smaller or shallower features on gravity maps compiled on a regional scale with those of deep-seated structures and geological materials. Hence, it is very important to compile Bouguer residual gravity anomaly map that predominantly reflect effects of local-scale or shallower features. The Bouguer Residual Gravity Anomaly Map Figure (4.5) is compiled by subtracting the upward continued gravity anomaly map Figure (4.4) values from the complete Bouguer gravity anomaly map Figure (4.3) values using the Geosoft software Oasis Montaj.

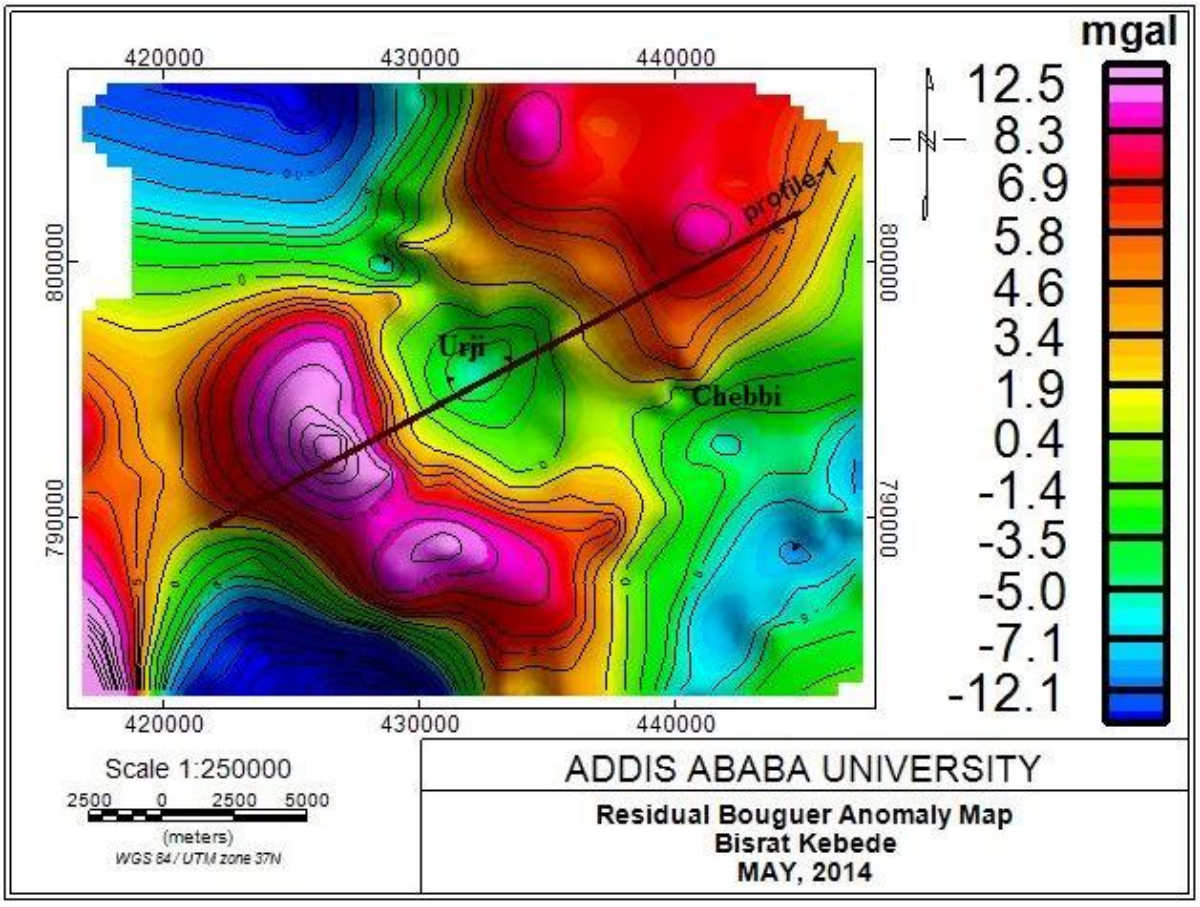

Figure 4.5 Bouguer residual gravity anomaly map of the Corbetti Caldera and its surrounding

The residual Bouguer gravity anomaly map Figure (4.5) of the study area generally varies locally from -14mgal up to 12mgal. Local positive and small negative gravity anomalies which are related to denser intrusions and low density materials are observed on the map.

On the residual Bouguer gravity anomaly map Figure (4.5), the circular negative gravity anomaly located at the center of the anomaly map outlines the Corbetti Caldera and the sharp gravity gradient flanking the circular negative anomaly outlines the rim of the Corbetti Caldera.

The Urji and Chebbi volcanoes are associated with local negative anomalies of about -6mgal. The cause for these negative anomalies may be the reflection of their higher elevations (2100m a.s.l). The other possible cause of these local negative anomalies over the elevated area of the Urji and Chebbi volcanoes may be interpreted as being caused by the rock types residing in the study area. Referring to the geologic map of the study area Figure (2.2) the Urji and Chebbi volcanoes are composed of thicker low density formation (pumice) as compared to the other parts of the caldera. These thick low density geological formations account for the observed local negative residual anomalies (-4mgal up to -7mgal). With the exception of the negative anomalies observed over the elevated areas, it may be considered that the whole caldera is within a positive local gravity anomaly.

The local positive gravity anomalies (9mgal-12mgal) in the study area are interpreted as being caused by a dense intrusion driven from the mantle to the crust by volcanic activity. The NW and SW parts of the caldera are associated with high negative anomalies (-12mgal up to -14mgal). According to the report of the MoME (1986), a geological structure (graben) with a thick infill of lake sediments and alluvium is assumed to be the cause of these local gravity lows.

4.3 Magnetic Method

4.3.1 Acquisition and Processing of magnetic data

The instrument used to collect the magnetic data is a proton precision magnetometer (IGS2) which measures the total intensity of the earth's magnetic field. Total field magnetic data were collected over random points and covering most of the areas over which the gravity and electrical VES were obtained as a secondary data from EGS. A total of about 200 data points were gathered with a station spacing of 500-1000 m. These data were then corrected for diurnal variations and unexpected data readings were removed from close examination of the data set. The magnetic anomaly is presented as total magnetic fields intensity and analytical signal anomaly map. As in the case of gravity, the magnetic anomaly map is prepared using Geosoft Ware Oasis Montaj. The end result of the magnetic work in the present study is a compilation of regional magnetic anomaly map that includes the area of interest, using the point magnetic anomaly values computed at each observation points and preparation of 2D-magnetic model constrained with 2D- gravity model and uses these results to obtain geological picture of the area under investigation. The analytical signal map is also prepared from regional magnetic anomaly map, and this method is very useful for delineating magnetic sources.

4.3.1.1 Total Magnetic Field Intensity Map

The total magnetic field intensity map shown in Figure (4.6), is prepared from the diurnal corrected magnetic data collected over the Corbetti Caldera and its surroundings. Referring to the total field magnetic anomaly map Figure (4.6) of the study area, the total field intensity values vary between 34600nT-35500nT and indicate the presence of prominent anomalous features.

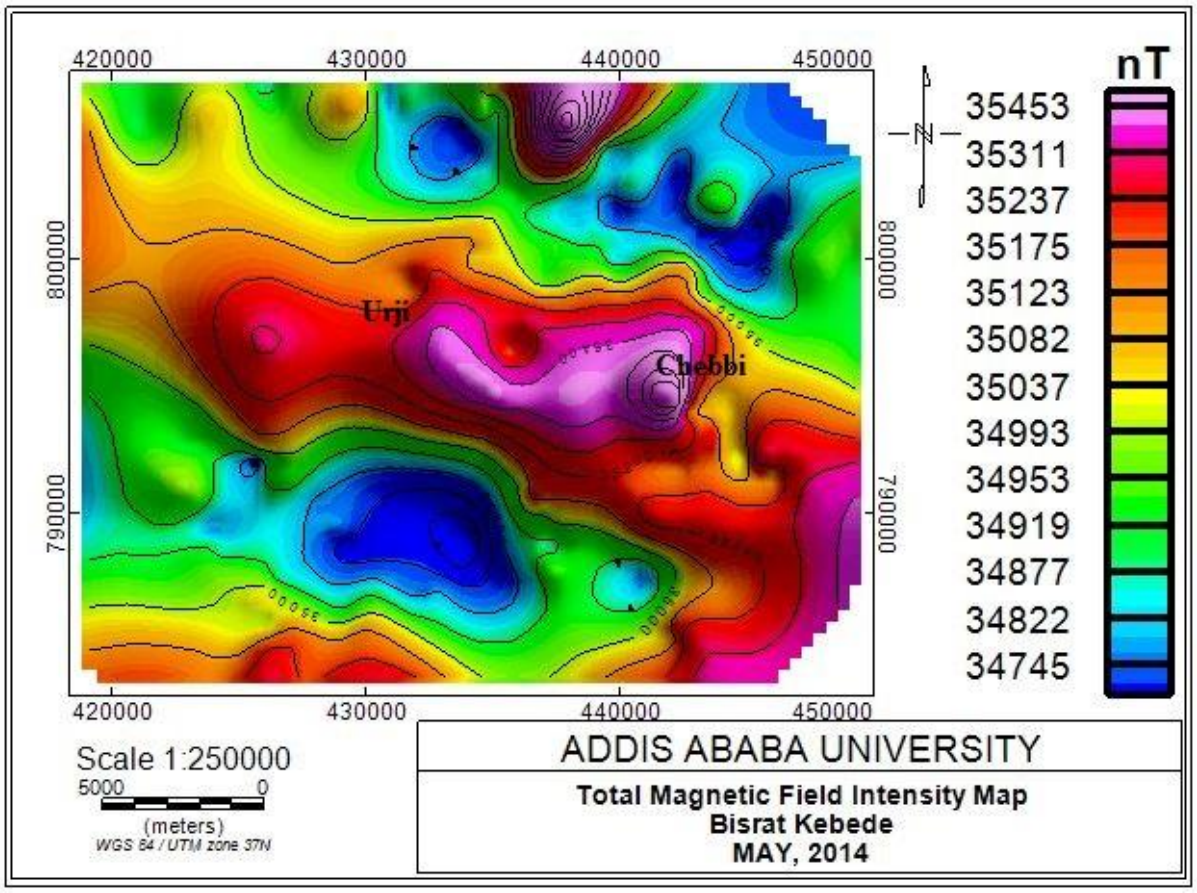

Figure 4.6 Total magnetic field intensity map of the Corbetti Caldera and its surroundings

On the total magnetic field intensity map, the region running from southeastern to northwestern parts of the study area along which the Chebbi and Urji volcanoes are located is associated with high total magnetic field intensity values. These maximum total magnetic field intensity values may be due to the existence of transversal E-W directed fissures which may form a zone of high mineralization generating the observed high magnetic values. On the other hand, the southwestern and northeastern parts of the caldera are associated with relatively lower total magnetic field intensity values where the Bouguer gravity anomaly map shows a maximum peak. The observed maximum gravity is interpreted as the effect the high density materials coming from the mantle during the formation of the nearby Corbetti caldera and post caldera activities. Correspondingly, the observed low total magnetic field intensity values may be interpreted as being generated relatively hot and high density intrusions which have lower magnetic susceptibility values due to their high heat content.

4.3.1.2 Magnetic Anomaly map

The magnetic anomaly map Figure (4.7) is generated by subtracting the IGRF value 35000nT from the observed magnetic data. Since the study area is very small the constant value (35000nT) subtracted represented represents the IGRF value of the whole study area considered.

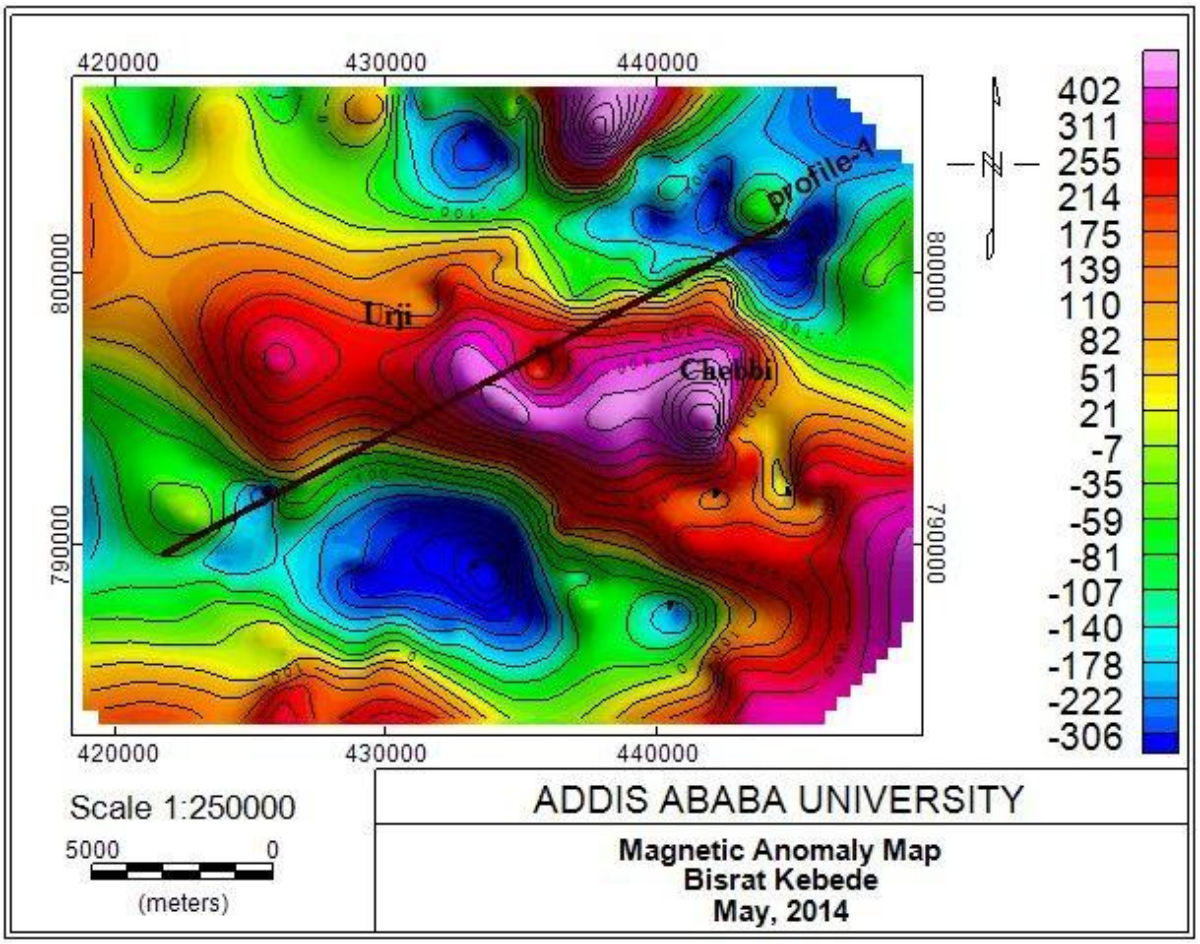

Figure 4.7 The Magnetic Anomaly Map of the Corbetti Caldera and its surroundings.

The magnetic anomaly map Figure (4.7) reflects the magnetic effects of subsurface rocks whose susceptibility varies laterally. The magnetic anomaly map almost coincide with the total magnetic field intensity map shown in Figure (4.6), this is because the IGRF value subtracted is considered to represents the regional magnetic effects of rock bodies associated with deep seated geologic structures.

4.3.1.3 Analytical Signal Map

Amplitude of the analytic signal can be defined as the square root of the squared sum of the vertical and the horizontal derivatives of the magnetic field, i.e.

$$B|(x,y,z)| = \sqrt{\left(\frac{\partial B}{\partial x}\right)^2 + \left(\frac{\partial B}{\partial y}\right)^2 + \left(\frac{\partial B}{\partial z}\right)^2} \qquad 4.1$$

where A is the amplitude and B is magnitude of the total magnetic field intensity.

The analytical signal is formed through a combination of horizontal and vertical gradients of the total magnetic field intensity and the method is very useful for delineating magnetic sources. The amplitude of a simple analytic signal indicates peaks over magnetic contacts (Nabighian, 1972). Therefore, the procedure can also be used to find location of horizontal contacts and depths of magnetic contacts. The analytic signal has a form over causative bodies that depend on the locations of the bodies but not their directions of magnetization.

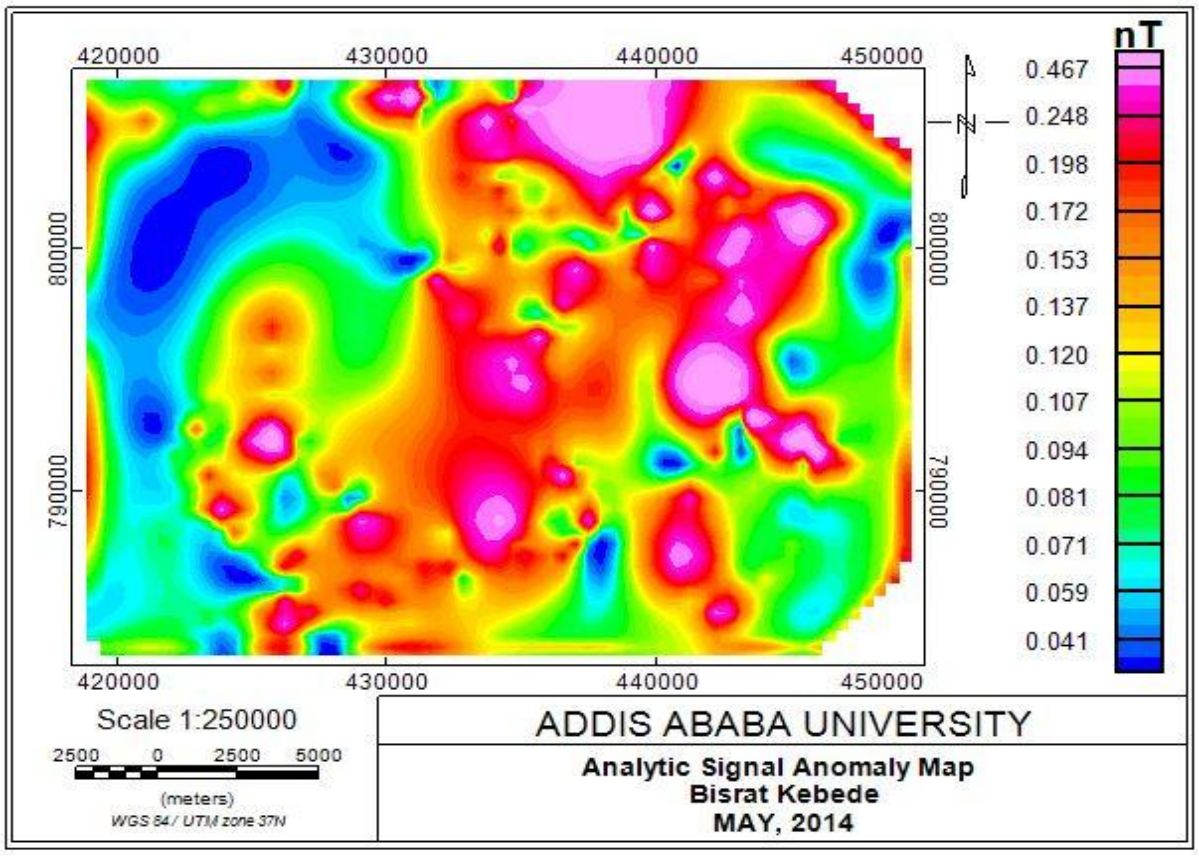

Figure 4.8 Analytic signal map of Corbetti Caldera and its surrounding.

The analytic signal map of the Corbetti caldera Figure (4.7) is produced from the total magnetic field map Figure (4.6). A close examination of the map confirms the existence of abnormal limiting (anomaly peaks). Medium anomaly peaks are observed over the Chebbi volcano and its surrounding. To the south of the Urji volcano the highest anomaly peaks are as shown on the map. High peaks are observed to the north of the Corbetti caldera rim containing the active thermal springs where the electrical resistivity maps Figure (4.9) show the lowest resistivity values over the study area.

4.4 Gravity and Magnetic Modeling

The forward modeling of the gravity and magnetic field has been done with gravity anomaly and total intensity values extracted along profile 1 shown on the residual Bouguer anomaly map Figure (4.5) and magnetic anomaly map Figure (4.7). The modeling is done with GM-SYS 5.01.10 software which is an extension of Geosoft OasisMontaj. The profile line (profile1) runs from southwest towards north east as shown both on the residual Bouguer gravity anomaly map and the magnetic anomaly map. The model shown in Figure (4.9) reflects a variety of structures with different lithology. The model produces a suitable fit of the calculated and the observed gravity data with (RMS) of 3.22mgal. The densities of the lithology have shown in the gravity model exhibits variations of approximately 10 – 15 %.

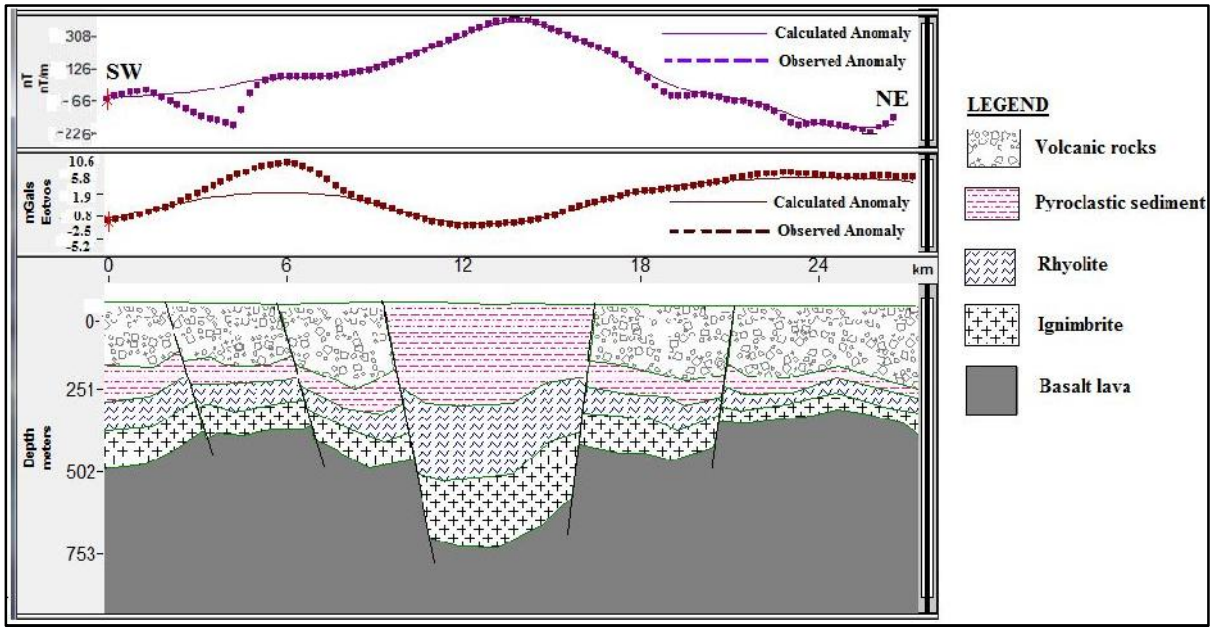

Figure 4.9 the Gravity and magnetic field modeling along the profile-1.

The magnetic and gravity field have identical profile line with an assumption that comparing and contrasting the two potential fields may give a better resolution of the geological and structural features of the Corbetti caldera along the profile. The susceptibility of the lithology shown in the magnetic model exhibits a variation of approximately 10 – 15 %.

Referring to the gravity and magnetic model in Figure (4.9) the top layer consists of volcanic rock of density 2.57g/cm^3 and magnetic susceptibility 0 – 0.43 with small variation of thickness approximately 140m-220m. The center of the caldera in which the Urji volcano is nested is filled with a pyroclastic sediments of density about 1.3 g/cm^3 and magnetic susceptibility ranging from 0.01 – 0.46, with an average thickness of 330m. The residual Bouguer gravity anomaly map Figure (4.5) clearly defines the geologic bodies (structures) below the Corbetti caldera with a circular negative anomaly overlying the Urji volcano and sharp anomaly gradients associated with the rim of the caldera. Thus the two middle faults in the gravity model indicate the caldera rim and the area between the two faults covered with thick pyroclastic deposit of the Corbetti caldera. The thin section which is overlaid by the volcanic rock at SW and NE of the caldera rim correspond to pyroclastic sediments with approximate thickness of 80 -100m and average density of 2g/cm^3. The layer underlain by the pyroclastic sediments is a rhyolite unit of density 2.52g/cm^3 which has a magnetic susceptibility range of 0.24 – 0.78. This rhyolite unit has a larger thickness (250 – 350m) within the Corbetti caldera and a smaller thickness (70 – 100m) to the SW and NE of the caldera. The ignimbrite rock overlying the basaltic bed rock has density value of 2.64g/cm^3 and magnetic susceptibility 0.27 – 0.69 with variable thickness ranging from 100 – 300m. The underlying basement consists of basaltic lava with a density value of 2.8g/cm^3 and magnetic susceptibility 0.25 – 0.75.

4.5 The Electrical Resistivity Method

4.5.1 Instrument and Data Acquisition

The electrical surveys were carried out by Geological Survey of Ethiopia (GSE), and all the VES data utilized in this thesis are secondary data from GSE. All 56 VES data point utilized in this project was collected by using Scintrex, 2.5kw instrument. The survey is carried out

along seven profiles in N-S orientation and some data points were randomly distributed over the study area. A total of 56 points has been taken using Schlumberger electrode array with the spacing between successive VES points of approxmation100m along the profiles. The electrode spacing (AB/2) of all VES points considered varies from 10m to 3160m.

4.5.2 Data Processing and Interpretation

One of the objectives of VES data interpretation is preparation of Shclumberger apparent resistivity map at a specific AB/2 for qualitative interpretations. The other objective of VES data interpretation is to determine the thicknesses and resistivities of different horizons by analyzing the resulting field curves to obtain the subsurface geological picture of the area under investigation. The computer modeling program (IP2WIN -inversion program) is used in this work for the determination of the final model parameters (thicknesses and resistivities) using Auto Cad-07.

4.5.2.1 Shclumberger Apparent Resistivity Map

The Shclumberger apparent resistivity map for AB/2=1810m and AB/2=2700m are prepared using geosoft OasisMontaj for qualitative interpretations. This involves determination of the special variation of the apparent resistivity over the study area at varying shallow depths.

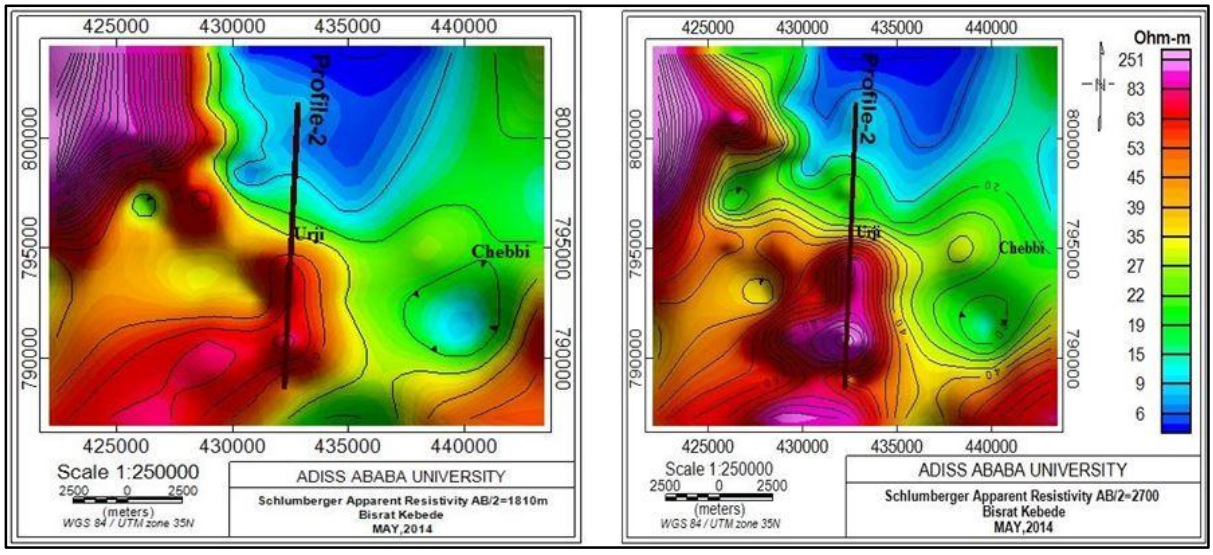

Figure 4.10 The Schlumberger apparent resistivity map for AB/2=1810m and AB/2=2700m

From the Schlumberger apparent resistivity map for AB/2=1810m and AB/2=2700m Figure (4.10), low resistivity anomaly follows the eastern and northern caldera rim, stretching north of the caldera towards Lake Shalla. Referring to the resistivity map AB/2=1810m, two areas that lie south and north of Chebbi and north of Urji are identified with a resistivity of 10Ω.m. A close observation of the anomaly map i.e., south and north of Chebbi, some 10Ω.m resistivity closures is indicated within this zone in the caldera although the effect of topography and shallower resistivity structures have canceled this low resistivity anomaly. A low resistive zone located north of the caldera in which the topographic effect considered to be small and cover relatively larger area with 10Ω.m can be interpreted as a thermally altered zone associated with the intrusive heat of the Corbetti caldera. Considering the apparent resistivity map for AB/2= 2700 we observe a sequential decrease in resistivity along the eastern parts of the caldera rim (from 80Ω.m to 7Ω.m) from south to the north. This low resistivity anomaly pattern is similar to the low resistivity anomaly pattern exhibited by the apparent resistivity map compiled for AB/2=1810m. Since Lake Awassa is at higher elevation (1680m a.s.l) than Lake Shalla (1570m a.s.l), this may show that the local hydrological situation is such that ground water flow is from south to the north across the Corbetti Caldera. Thus this ground water flowing across the caldera interacts with the intrusive heat coming from the Corbetti caldera contributing to the sequential decrease of the resistivity from south to north. The existing supporting evidence of the presence of hot springs on the southern shore of Lake Shalla could mean a contribution the Corbetti caldera to provide the hot fluid of the Shalla system. The other existing evidence is the absence of thermal features south of the Corbetti caldera or north of Lake Awasa which also stands as a clue to predict the migration of hot water from the caldera to Lake Shalla that gives rise to the observed sequential decrease of the apparent resistivity from south to north.

4.5.2.2 Apparent resistivity Pseudo depth-section

Pseudo-section along Profile-2 which is shown in Figure (4.11) is constructed from the apparent resistivity values using mapping software “surfer 8”. It qualitatively shows the lateral and vertical variations of the electrical properties of the subsurface geologic bodies. The VES profile is selected for the simple reason that it traverses the caldera from south to

north and crosses the Urji volcano deemed to reflect a better geological condition associated with the resistivity of the formation related to the geothermal aspects of the study area.

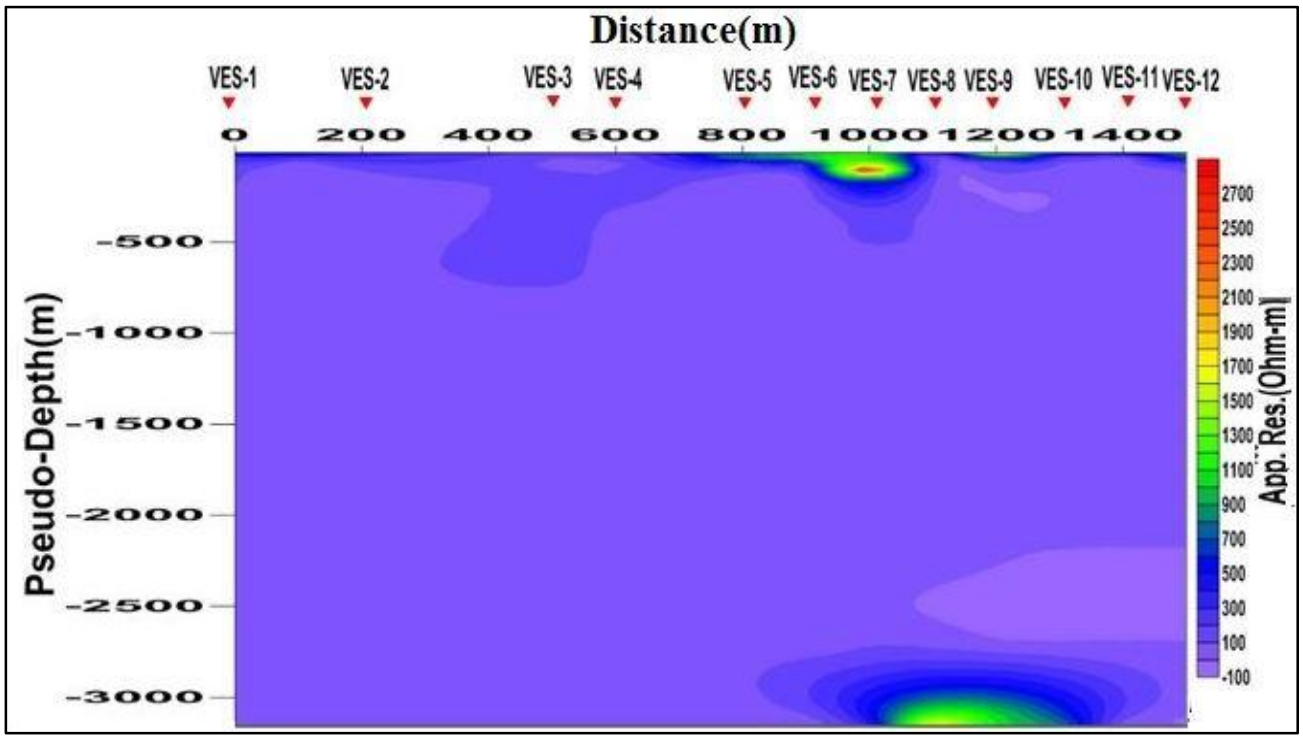

Figure 4.11 Electrical resistivity pseudo-depth section along Profile-2

The profile line in which Pseudo-section is constructed traverses the Corbetti caldera especially the Urji volcano in S-N direction. A resistive overburden of thin layer occupies the top of the section and is underlain by relatively conductive substratum. A resistive overburden of thin layer occupies the top of the section from VES-1 up to VES-5 that shows an elongation at VES-3 andVES-4. Starting from VES-5 a highly resistive overburden of thin layer occupies the top of the section which is elongated gradually down ward up to VES-8 and it appears as a thin at VES-9. VES-9, VES-10, VES-11 and VES-12 are of a top of the section highly resistive overburden of thin layer. Generally the Pseudo-section shown on Figure (4.11) exhibits a thick middle conductive zone

4.5.2.3. Interpreted Curve and Geoelectric Section along Profile-2

There are twelve VES data points (VES-1, VES-2 … VES-12) along the profile and each of the VES points were inverted using IP2WIN. The inverted curves show 5-7 geoelectric layers

with a minimum error of 4-9%. The geoelctric layers compiled for VES-9 and VES-10 are shown in Figure (4.12). The geoelctric layers compiled for the remaining VES points are shown in Appendix I.

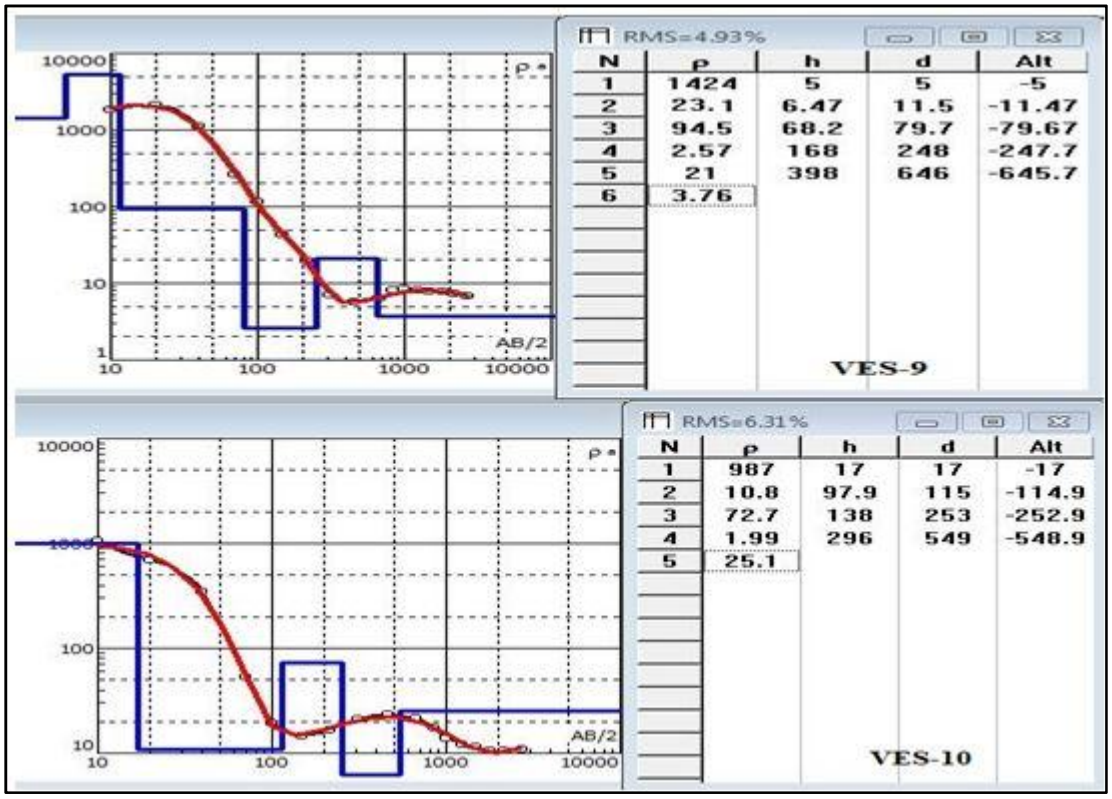

Figure 4.12 VES-9 and VES-10 interpreted curves

Both the resistivity curve shown in Figure (4.12), show higher resistivity at the top layer and a gradual decrease of resistivity observed in both curves as the depth increases. The two curves are selected as a sample out of the twelve curves on the basis of curves showing very minimum resistivitys. In fact, all the curves somehow exhibit the properties of the two curves chosen as a sample.

The geoelectric section shown in Figure (4.13) is prepared from the interpreted curves using Auto Cad-07. The geoelectric section generally separated into three parts described as follows:

The top layer in which its resistivity varies from 80Ω.m - 2750Ω.m, in which its thickness increases from 50m – 350m from Urji volcano to the northern parts of the caldera. Referring to the geologic map the Urji volcano approximately located under VES-4-VES-10 covered with thicker low density formation (pumice) up to 350m depth at the top layer and 50m – 100m thick under VES-1, VES-2, VES-3, VES -11 and VES-12 is lake sediments and alluvium.

The middle conductive zone which acquires a very low resistivity from 0.56Ω.m - 75Ω.m with a variable thickness 200m - 900m, one of the reasons for resistivity to decrease is the increase in temperature, the other reason for the decrease of resistivity of rocks is the assemblage of conductive minerals due to alteration.

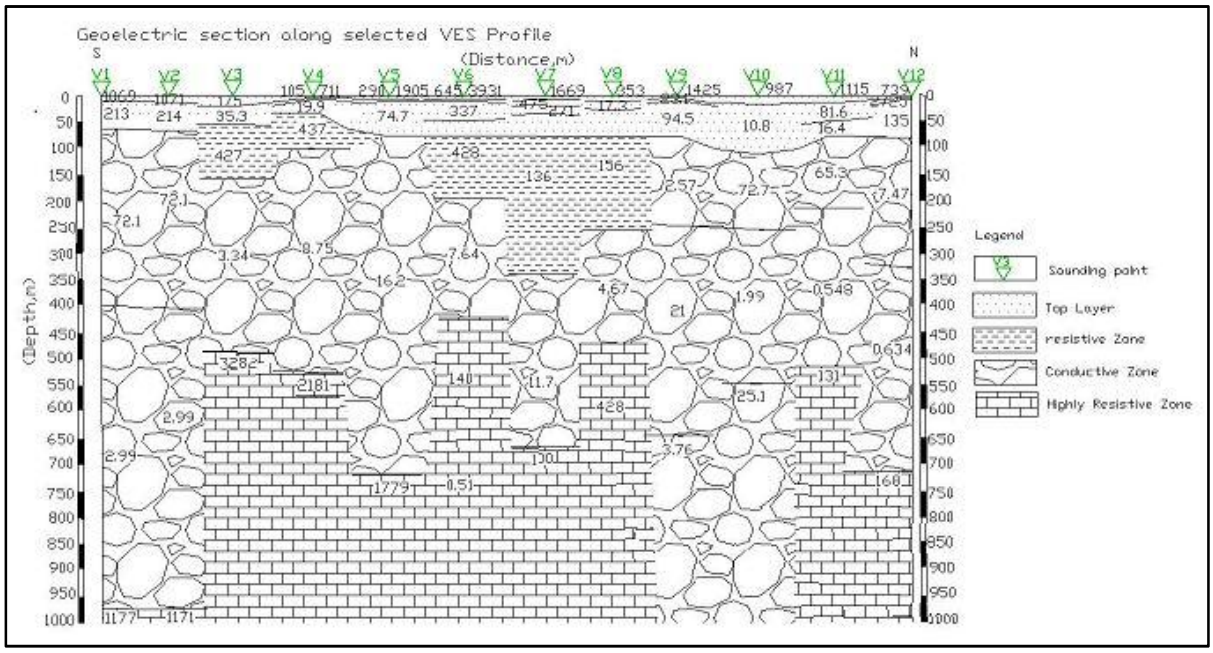

Figure 4.13 The Geoelectric section along profile-2

The bottom highly resistive zone in which its resistivity varies from 100Ω.m - 3290Ω.m having a variable thickness from 50m – 550m may be interpreted as Rhyolite and Basalt lava which is common in the area.

CHAPTER FIVE

5 CONCLUSIONS AND RECOMMENDATIONS

5.1 Conclusions

Corbetti caldera is associated with a high gravity field with slight modifications by the product of Chebi and Urji volcanoes which relatively exhibit low gravity field in the vicinity of the study area. This is due to the fact that the Corbetti caldera consists of mantle materials of large denser intrusion which comes to the crust during the volcanic activities.

The very high local as well as regional Bouguer gravity anomalies indicate the existence of intrusions at shallow and deeper depths beneath the caldera. When comparing the Bouguer anomaly and total intensity map, we observe areas with very high gravity anomalies to show very low total magnetic field intensity values. Hence, it seems that the intrusive bodies act as sources of heat beneath the study area, i.e., due to the very high heat which is generated by the intrusive rocks seem to lose their magnetic susceptibility. The local Bouguer gravity anomalies clearly define the caldera with a circular gravity anomaly and the caldera rim with sharp gradient of the local gravity anomaly.

The Schlumberger apparent resistivity map for AB/2=1810m and AB/2=2700m shows low resistivity anomaly over the eastern and northern caldera rim and stretching north of the caldera towards Lake Shalla, this sequential decrease of the resistivity along the eastern parts of the caldera rim from 50Ω.m to 4Ω.m in the direction of south to north, with the absence of the thermal features south of the Corbetti caldera and hot springs on the southern shore of Lake Shalla is a clue to predict that the hot water migrates from the Corbetti caldera to Lake Shalla, i.e., the ground water flowes from Lake Awassa to Lake Shalla interacts with the intrusive heat of the Corrbetti caldera at the middle of the two Lakes thus, the hot fluid of the Shalla system could mean a contribution from the Corbetti caldera.

The apparent resistivity pseudo sections and the true resistivity geoelectric sections show the presence middle thicker conductive zone which is associated with the increase in temperature and alteration.

The forward modeling of the magnetic and gravity data show the presence of structures along the modeled profile line and these structures are aligned in the general direction of rift axis (Southeast- Northwest direction)

The geophysical data used in this research is very restricted to the study area due to limitation of resources. Based on the joint analysis of these geophysical data and the existing dominant thermal manifestations toward the northern parts of the Corbetti caldera the study area in which the Urji and Chebbi volcanoes are nested toward the southern shores of Lake Shalla has large scale geothermal potential for further development from centre of caldera.

5.2 Recommendation

Based on the results obtained and the limitation of this research the following points are recommended.

- Adequate coverage of the area by gravity and magnetic data can provide additional information to facilitate the complete understanding and planning for future exploitation of the geothermal and possibly the epithermal resources associated with the Corbetti caldera.

- Magneto-telluric (MT) methods are recommended for Corrbetti caldera, for their potential to probe large depths and enhanced capacity in delineating subsurface horizons of anomalous heat and/or fluid flow.

- Integrating the geophysical results obtained with hydro geological, geochemistry and heat flow model is very crucial before qualifying the area for large-scale usage of geothermal resources.

REFERENCES AND BIBLOGRAPHY

Baker, J., Snee, L., Menzies, M., 1996. A brief Oligocene period of flood volcanism in Yemen. Earth Planet. Sci. Lett. **138**: 39–55.

Bastow, I.D., Stuart, G.W., Kendall, J.-M., Ebinger, C.J., 2005.Upper mantle seismic structure in a region of incipient continental breakup: northern Ethiopian rift. Geophys. J. Int. **162**: 479–493.

Benoit, M.H., Nyblade, A.A., VanDecar, J.C., 2006. Upper mantle P-wave speed variations beneath Ethiopia and the origin of the Afar hotspot. Geology **34**: 329–332.

Bonini, M., Corti, G., Innocenti, F., Manetti, P., Mazzarini, F., Abebe, T., Pecskay, Z., 2005. Evolution of the Main Ethiopian Rift in the frame of Afar and Kenya rifts propagation. Tectonics 24, TC1007. doi:10.1029/2004TC001680

Chernet, T., Hart, W., Aronson, J., Walter, R.C., 1998. New age constraints on the timing of volcanism and tectonism in the northern Main Ethiopian Rift — southern Afar transition zone (Ethiopia). J. Volcanol. Geotherm. Res. **80**: 267–280.

Church, W.R., 1991. Discussion of "Ophiolites in northeast and East Africa: implications for Proterozoic crustal growth". J. Geol. Soc. (Lond.) **48**: 600–606.

Di Paola, G.M., 1975. The Ethiopian Rift Valley (between 7 and 8 or 40E Lat. North) Bull. **36**: 517-542.

Dobrin, M.B.,and Savit,C.H., 1988. Introduction to geophysical prospecting. MCGraw. Hill Inc. Singapore.

Ebinger, C.J.,Yemane, Giday WoldeGabriel, Aronson, J.L.,Walter,R.C., 1993. Late Eocene—recent volcanism and faulting in the southern main Ethiopian rift. J. Geol. Soc. (Lond.) **150**: 99–108.

Ebinger,C.,Yemane, T.,Harding,D., Tesfaye, S.,Rex,D., Kelley, S., 2000. Rift deflection, migration, and propagation: linkage of the Ethiopian and Eastern rifts, Africa. Geol. Soc. Amer. Bull. **102**: 163–176.England.

Altaye,E., Oluma,B., Hunegenaw,A., Tadesse,K., Abdulkadir,M., 1983. Geological Report of Corbetti Area on 1:50,000 scale Ethiopian Geothermal Exploration Project, Ministry of Mines and Energy, Addis Ababa.

Altaye,E, 1984. Geology and Surface Alteration of the Cobetti caldera Area, University of Auckkland, New Zealand, report pp. 71.

George, R., Rogers, N., 2002. Plume dynamics beneath the African plate inferred from the geochemistry of the Tertiary basalts of southern Ethiopia. Contrib. Mineral. Petrol. **144**: 286–304

Hofmann,C., Courtillot,V., Feraud,G., Rochette, P., Yirgu, G.,Ketefo, E., Pik, R., 1997. Timing of the Ethiopian flood basalt event: implications for plume birth and global change. Nature **389**: 838–841.

John M. Reynolds 1997. An Introduction to Applied & Enviromental Geophysics. John Willey & sons Ltd, England, pp 32 -118.

Locke, C.A. and de Ronde, C.E.J., 1987. Delineation of gold bearing hydrothermally altered rocks using gravity data -New Zealand example. Geoexploration, **24**: 471-481.

LIoyd, E. F., 1977. Geological Factors Influencing Geothermal Exploration in the Langano Region, Ethiopia, NZ Geological survey, Rotorua, New Zealand, Unpublished Report. pp.73.

Macdonald, R., and Gibson, I.L., 1969: Pantelleritic obsidian from the Volcano Chebbi (Ethiopia), contr. Min. petrol. 24, p 239 – 244.

Martin, F., Don, R., and Rosa-Lee, B., 1976. A Gravity and Magnetic Investigation of the Long Valley Cadera, Mono County, California. JGR, **81:754**-762.

Mohr, P.A., 1962b. Geological report on the Lake Langano and adjacent plateau regions. Bull Geoph. Obs. Addis Ababa, **9**: 59-75.

Mohr, P.A., 1966: Chebbi Volcano (Ethiopia), bull.volcanol, 29, p797 – 810.

MoME, 2011. Report on Results of Near Surface Temperature Measurments and Associated Hydrothermal Alteration Studies In Corbetti Geothermal Prospect, Ethiopia Project Profile, Addis Ababa.

MoME, 2008. Investment opportunities in geothermal energy development Corbetti geothermal prospect, Ethiopia Project Profile, Addis Ababa; 38-45

MoME., 1986. Geothermal exploration project lake district, Corbetti geothermal prospect geophysical exploration, Ethiopia Project Profile, Addis Ababa.

Montelli,R., Nolet, G.,Dahlen, F.A.,Masters,G., 2006.Acatalogue of deep mantle plumes: new results from finite frequency tomography. Geochem. Geophys.Geosyst. 7,Q11007. doi:**10**.1029/2006GC001248.

Nabighian. M.N., 1972. The analytic signal of two-dimensional magneticbodies with polygonal cross section: its properties and use forautomated anomaly interpretation. Geophysics,**37**,507-517.

Palmasson ,G,. 1975. Geophysical methods in geo thermal exploration. Proceedings of the second UN symposium on the development and uses of geothermal resources. San Francisco, **2**: 161-200.

Reynolds, J.M., 1997: An introduction to applied and environmental geophysics. John Wiley and Sons, NY, pp: 806.

Telford, W.M., Sheriff, R.E., and Geldart, L.P., 1990. Applied Geophysics. Second edition Cambrdge.

Ukstins, I., Renne, P., Wolfenden, E., Baker, J., Menzies, M., 2002. Matching conjugate volcanic rifted margins: 40Ar/39Ar chrono-stratigraphy of pre- and syn-rift bimodal flood volcanism in Ethiopia and Yemen. Earth Planet. Sci. Lett. **198:** 289–306.

UNDP, 1973 Technical report, Investigation of Geothermal Recourses for Power Development of the East African Rift system In Ethiopia, NEW YORK.

Giday WoldeGabriel., Aronson, J., Walter, R., 1990. Geology, geochronology, and rift basin development in the central sector of the Main Ethiopian rift. Geol. Soc. Am. Bull. **102**: 439–458.

Giday WoldeGabriel., Yemane, T., White, T., Asfaw, B., Suwa, G., 1991. Age of volcanism and fossils in the Burji–Soyoma area, Amaro Horst, southern Main Ethiopian Rift. J. Afr. Earth Sci. **13**: 437–447.

Wolfenden, E., Ebinger, C., Yirgu, G., Deino, A., Ayalew, D., 2004. Evolution of the northern Main Ethiopian rift: birth of a triple junction. Earth Planet. Sci. Lett. **224**: 213–228.

APPENDIX -I

Pseudo depth section prepared by Ip2 WIN

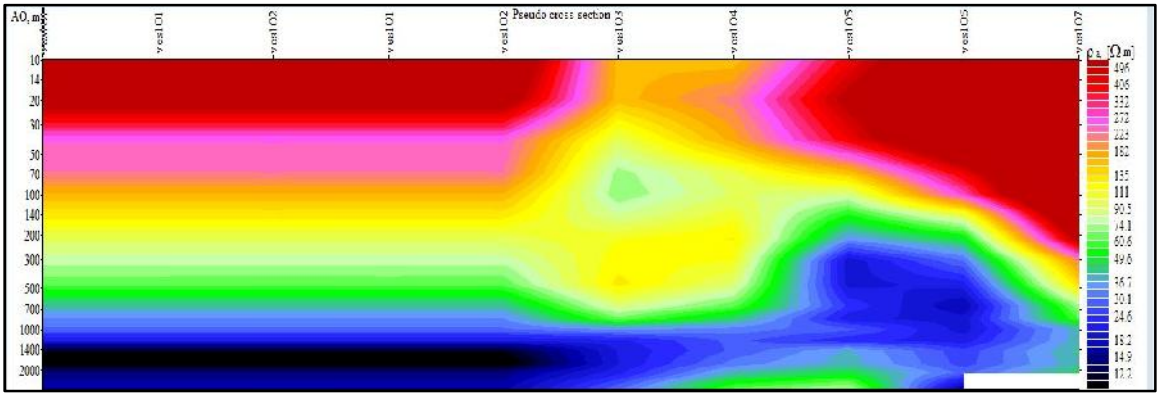

Interpreted Cureves of VES Along The profile